

---

# CreFlow: Corrective Reflow for Sparse-Reward Embodied Video Diffusion RL

---

Zhenyang Ni<sup>1</sup> Yijiang Li<sup>2</sup> Ruochen Jiao<sup>1</sup> Simon Sinong Zhan<sup>1</sup> Sipeng Chen<sup>1</sup>

Zhenfei Yin<sup>3</sup> Minshuo Chen<sup>1</sup> Philip Torr<sup>3</sup> Zhaoran Wang<sup>1</sup> Qi Zhu<sup>1</sup>

<sup>1</sup>Northwestern University <sup>2</sup>University of California, San Diego <sup>3</sup>University of Oxford

## Abstract

Video generation models trained on heterogeneous data with likelihood-surrogate objectives can produce visually plausible rollouts that violate physical constraints in embodied manipulation. Although reinforcement-learning post-training offers a natural route to adapting VGMs, existing video-RL rewards often reduce each rollout to a low-level visual metric, whereas manipulation video evaluation requires logic-based verification of whether the rollout satisfies a compositional task specification. To fill this gap, we introduce a compositional constraint-based reward model for post-training embodied video generation models, which automatically formulates task requirements as a composition of Linear Temporal Logic constraints, providing faithful rewards and localized error information in generated videos. To achieve effective improvement in high-dimensional video generation using these reward signals, we further propose CreFlow, a novel online RL framework with two key designs: i) a credit-aware NFT loss that confines the RL update to reward-relevant regions, preventing perturbations to unrelated regions during post-training; and ii) a corrective reflow loss that leverages within-group positive samples as an explicit estimate of the correction direction, stabilizing and accelerating training. Experiments show that CreFlow yields reward judgments better aligned with human and simulator success labels than existing methods and improves downstream execution success by 23.8 percentage points across eight bimanual manipulation tasks.

## 1 Introduction

A growing body of work has explored the integration of video generation models (VGMs) into robotic manipulation systems [12, 6, 10, 2, 14, 30]. Despite their impressive perceptual fidelity, videos synthesized by modern VGMs still suffer from physical implausibility in embodied manipulation. This limitation stems from both data and objective mismatches: web-scale pretraining data include heterogeneous sources such as entertainment videos that may violate physical rules, while likelihood-surrogate objectives [15] treat pixels uniformly and favor global plausibility over task-critical robot-object interactions. To mitigate these limitations, recent studies have used reinforcement learning to align general-purpose VGMs with specific reward targets, including visual quality [35], scene-level 3D consistency [11], and action executability [34].

Despite these promising efforts, reward design for manipulation video RL remains substantially more demanding than generic video evaluation. A generated video may appear globally coherent while still containing subtle pixel-level errors that will lead to inaccurate actions and compounding failures over time [15]; see Fig. 1. Targeting single aspects of video quality [35, 34], existing video RL rewards are prone to missing such small but decisive violations, since the reward for evaluating manipulation

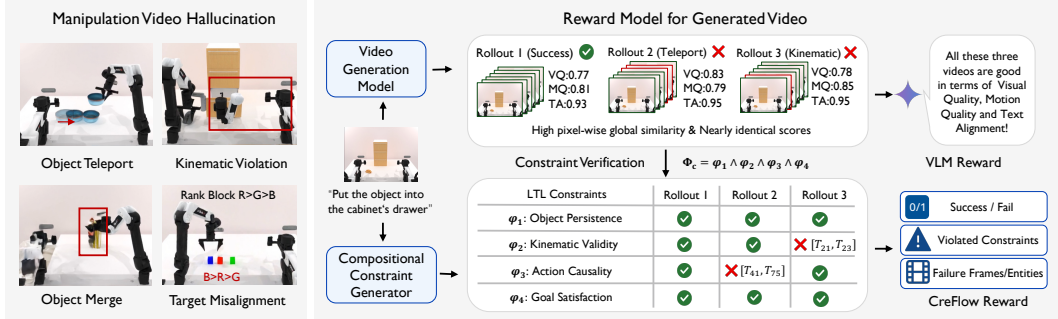


Figure 1: Generated manipulation videos can be nearly indistinguishable under existing reward models [23, 35], yet differ critically in downstream robot execution. This ambiguity arises from two properties of manipulation videos: the decisive error may occupy only a small spatio-temporal region, and correctness depends on logic-based verification of compositional robot–object constraints rather than low-level visual quality alone. CreFlow evaluates rollouts with compositional LTL constraints  $\Phi_c$ , producing a faithful binary success signal together with localized violation traces over constraints, frames, and entities, providing faithful and informative signal for RL post-training.

videos is naturally compositional [40]: multiple requirements must be satisfied simultaneously for task execution to succeed. For example, in a put-object-into-cabinet-drawer task, the object must persist throughout the video, the robot motion must remain kinematically valid, and the object must be placed inside the target drawer with correct action causality (drawer should not open without a robot grasping it). Moreover, even a faithful reward signal—whose verdict reflects downstream task success—is insufficient, as high-dimensional video rollouts are dominated by reward-irrelevant pixels and time intervals. Uniformly applying RL updates to the full video therefore wastes gradient on these areas, perturbing regions that are already plausible or unrelated to downstream execution.

To fill this gap, we introduce a compositional constraint-based reward model for post-training embodied video generation models, which provides not only faithful reward that evaluates downstream task success possibility, but also diagnostic signals that expose where and why a rollout fails. To realize this, our core idea is to automatically formulate task success as a set of Linear Temporal Logic (LTL) constraints, where each constraint encodes an atomic requirement, and their composition jointly represents the holistic evaluation objective. Each LTL constraint is evaluated over robot and object state traces, capturing the causal logic in the generated videos and providing spatio-temporal diagnostic information for locating the violation. The constraint generation process is implemented by a coding agent, which leverages low-level vision modules to extract the states needed for constraint evaluation, including SAM3 [5], VLM [31], and IDM [14, 30].

Following this strategy, we propose Corrective Reflow (CreFlow), an online RL framework that converts compositional constraint violations into localized corrective objectives for manipulation video diffusion models. CreFlow introduces two key designs for turning sparse task failures into actionable supervision. First, it aggregates the per-rollout violation traces in a group into a spatio-temporal mask over the responsible entities and frames, and applies a credit-aware NFT loss that confines the positive–negative velocity contrast to reward-relevant regions. This prevents sparse task feedback from perturbing irrelevant pixels and keeps non-violating regions anchored to the pretrained video prior. Second, for each failed rollout, CreFlow aggregates the within-group successful rollouts generated under the same initial observation and instruction, and uses their mean aggregation as an explicit corrective target rather than merely suppressing the generation probability of negative samples. Together, these training objectives provide a more effective way to leverage both constraint-based reward feedback and relative information among rollouts generated under the same condition.

The contributions of this work are summarized as follows: i) We introduce a compositional constraint-based reward model that evaluates embodied video generation with automatically generated LTL constraints, providing not only faithful reward but also localized diagnostics for subtle rollout errors. ii) We propose CreFlow, a novel video RL framework that turns sparse compositional violations into a localized corrective estimator, combining a credit-aware NFT loss and a corrective reflow loss to deliver focused, low-variance updates on task-critical regions. iii) Extensive experiments on eight RoboTwin tasks show that CreFlow yields reward judgments better aligned with human and simulator success labels than existing methods, leads to effective training to improve high dimensional video generation, and improves downstream execution success by 23.8 percentage points.

## 2 Related Work

**Video Generation Model for Robot Manipulation.** Video generative models (VGMs) have emerged as a promising foundation for robotic manipulation [12, 13, 2, 16, 10, 6, 14, 3, 24, 38]. Most methods follow a two-stage pipeline: generating a video plan from the task instruction and current observation, and then retargeting the predicted motion into robot actions via inverse dynamics models (IDMs). Recent progress has improved both physically plausible video prediction [6, 1, 8] and general-purpose IDMs [14, 30]. However, a fundamental gap remains between generating globally coherent videos and producing robot actions that can be successfully executed in the physical world [15, 34]. While EmboAlign [40] uses compositional constraints to filter implausible videos before action retargeting, our work focuses on improving the VGM itself through constraint-guided post-training.

**Reward Modeling for Video Generation.** Designing effective rewards for video generation is challenging because task-relevant failures may be sparse in space and time. Existing video reward models either adapt image-level metrics such as CLIP and human preference scores [32, 28, 25], or learn preference rewards for visual quality, motion quality, and text alignment [23]. For physical applications, recent methods further evaluate specific properties such as 3D consistency [11], action smoothness and reachability [34], or visual distortions [8]. Nevertheless, these rewards remain insufficient for manipulation videos, where downstream success depends on compositional requirements and subtle robot-object interactions. Inspired by constraint-based task specifications [40, 17, 43, 9], we formulate manipulation success as LTL-style temporal compositions over continuous predicates, enabling faithful success evaluation and localized failure diagnosis.

**Reinforcement Learning and Preference Alignment for Video Generation.** Reinforcement learning and preference alignment have become important tools for adapting generative models to objectives beyond likelihood-based pretraining. Existing post-training methods for flow or diffusion VGMs largely inherit image-generation RL strategies, including policy-gradient training with stochastic samplers [37, 22, 20] and reward-weighted denoising objectives such as Diffusion-NFT [41]. Recent video-oriented methods [32, 42] further show that directly applying image-level objectives to videos can underuse within-condition sample relationships and introduce unstable latent perturbations. Manipulation video generation amplifies these challenges, since reliable dense rewards are unavailable, subtle pixel-level errors can determine downstream execution, and most pixels are irrelevant to the actual failure. To address this, CreFlow turns sparse-reward video diffusion RL into a localized corrective estimator: violation traces from the constraint monitor confine the reward-induced gradient to failure-relevant regions, and the corrective reflow loss replaces the symmetric reflection target used by negative-aware finetuning [41] with a distributional anchor toward the within-condition positive marginal, estimated by the empirical mean of within-group successful rollouts.

## 3 Problem Formulation and Preliminaries

**Video policy and objective.** We study online reinforcement-learning post-training of a pretrained flow-matching text-image-to-video (TI2V) model for robot manipulation. Let  $y = (c, \mathbf{I}) \sim \mathcal{D}_{\text{task}}$  denote a task context, where  $c$  is the language instruction and  $\mathbf{I}$  is the first-frame observation. Following the video-as-policy pipeline of Vidar [14], a trainable video generator samples a rollout  $\mathbf{x}_0 \sim p_{\theta}(\cdot | y)$ , and a frozen inverse-dynamics decoder  $\mathcal{I}_{\text{IDM}}$  maps the rollout to robot actions  $\mathbf{a} = \mathcal{I}_{\text{IDM}}(\mathbf{x}_0)$ . Only the video generator parameters  $\theta$  are updated during post-training.

Let  $\text{Succ}(\mathbf{a}; y) \in \{0, 1\}$  be the binary indicator of successful execution in the target environment. The ideal objective is

$$J_{\text{succ}}(\theta) = \mathbb{E}_{y \sim \mathcal{D}_{\text{task}}} \mathbb{E}_{\mathbf{x}_0 \sim p_{\theta}(\cdot | y)} [\text{Succ}(\mathcal{I}_{\text{IDM}}(\mathbf{x}_0); y)]. \quad (1)$$

Evaluating  $\text{Succ}$  requires executing decoded actions on a real robot or high-fidelity simulator, so it is too expensive for the inner training loop. During post-training, we instead score generated rollouts with the compositional constraint introduced in Sec. 4.1.

**DiffusionNFT surrogate.** CreFlow builds on the DiffusionNFT [41] surrogate for online reinforcement learning of diffusion or flow models. In each online iteration, we sample rollouts from the behavior policy  $p_{\theta_{\text{old}}}(\cdot | y)$  and use  $i$  to index samples in this rollout batch. For each  $\mathbf{x}_0^{(i)}$ , draw  $t \sim \mathcal{U}[0, 1]$  and  $\epsilon \sim \mathcal{N}(0, I)$ , and use the rectified-flow interpolation

$$\mathbf{x}_t^{(i)} = (1 - t)\mathbf{x}_0^{(i)} + t\epsilon, \quad \mathbf{v}^{(i)} = \epsilon - \mathbf{x}_0^{(i)}. \quad (2)$$

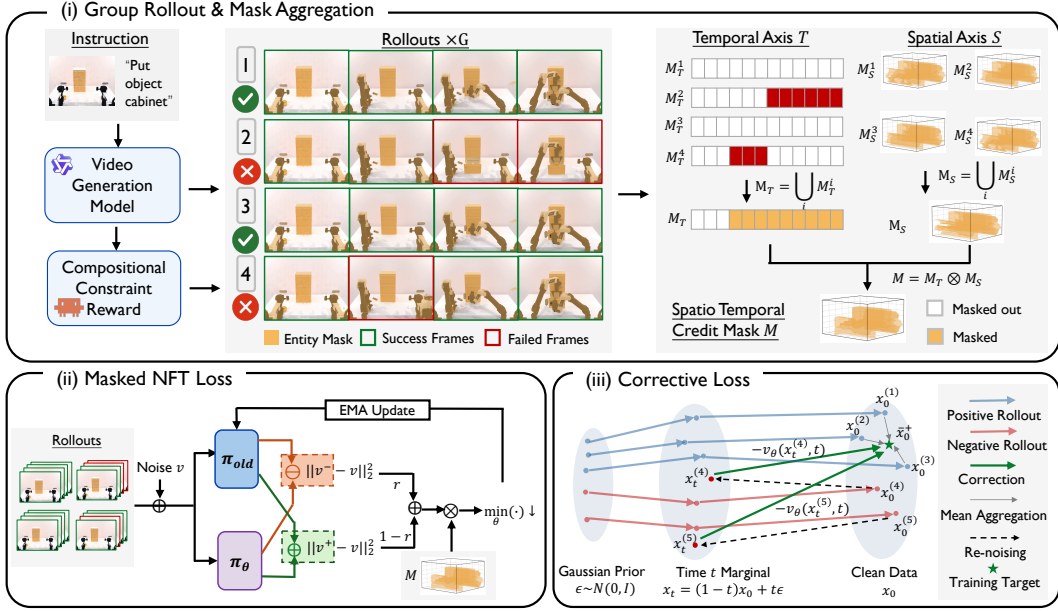


Figure 2: **Overview of CreFlow.** CreFlow turns sparse compositional reward feedback into localized supervision for video diffusion post-training. Instead of applying reward-induced updates uniformly over the full rollout, it identifies the spatio-temporal mask responsible for task success or failure and restricts optimization to these regions. The resulting objective combines localized negative-aware finetuning with an explicit corrective target from same-condition successful rollouts, enabling stable improvement under sparse binary manipulation rewards.

Let  $v_\theta$  be the trainable velocity field and  $v_{\text{old}} = \text{sg}(v_{\theta_{\text{old}}})$  be the stop-gradient behavior velocity. DiffusionNFT defines positive and negative branches

$$v_\theta^+ = (1 - \beta)v_{\text{old}} + \beta v_\theta, \quad v_\theta^- = (1 + \beta)v_{\text{old}} - \beta v_\theta, \quad (3)$$

where  $\beta > 0$  controls the reinforcement strength. Its loss is

$$\mathcal{L}_{\text{NFT}}(\theta) = \mathbb{E}_{y, i, t, \epsilon} \left[ r_i \|v_\theta^+(\mathbf{x}_t^{(i)}, t, y) - \mathbf{v}^+\|_2^2 + (1 - r_i) \|v_\theta^-(\mathbf{x}_t^{(i)}, t, y) - \mathbf{v}^-\|_2^2 \right], \quad (4)$$

where  $r_i \in \{0, 1\}$  denotes the reward of rollout  $\mathbf{x}_0^{(i)}$ . Intuitively,  $\mathcal{L}_{\text{NFT}}$  performs implicit preference learning: the  $r_i = 1$  branch reduces to a rejection-style [19] flow-matching update on successful rollouts, while the  $r_i = 0$  branch keeps  $v_{\text{old}}$  as an anchor and trains  $v_\theta$  toward the reflected target of a failed rollout, thereby pushing the policy away from low-reward samples rather than simply discarding them.

## 4 Method

This section presents CreFlow, an online RL framework that converts compositional task violations into localized corrective updates for post-training manipulation VGMs; see Fig. 2. The key challenge is not only to obtain a faithful success signal, but also to make this sparse binary signal usable for optimizing high-dimensional video rollouts. CreFlow first evaluates each rollout with a task-specific finite-trace LTL monitor (§4.1), which verifies a compositional task specification and returns both a binary success label and violation traces over constraints, entities, and frames. It then uses these traces to build two localized objectives: a group-shared credit-aware NFT loss (§4.2) that restricts negative-aware finetuning to reward-relevant spatio-temporal regions, and a corrective reflow loss (§4.3) that pulls failed rollouts toward the empirical mean of same-condition successful rollouts on their violated regions.

### 4.1 Compositional Constraint Monitor

Existing video reward models for embodied generation either reduce a rollout to a single quality dimension [35, 23, 32] or rely on a VLM-as-judge that subsamples a few frames and overlooks the

small objects and short-window events on which manipulation success actually pivots [8]. Manipulation success, by contrast, is compositional: several temporal and causal conditions must hold jointly throughout a rollout. Inspired by recent work that specifies embodied task goals and safety with Temporal Logic specification [39, 21], CreFlow introduces a compositional constraint monitor  $\mathcal{M}_c$  that lifts each rollout into a perception-grounded state trace, evaluates a conjunction of finite-trace Linear Temporal Logic clauses, and returns

$$(r, \mathcal{V}, \mathcal{S}) = \mathcal{M}_c(x_0; y), \quad (5)$$

where  $r \in \{0, 1\}$  surrogates Succ in Eq. (1),  $\mathcal{V}$  is the per-clause violation record, and  $\mathcal{S}$  is the per-entity SAM3 mask atlas. Together  $(\mathcal{V}, \mathcal{S})$  encode *when* and *where* the rollout’s behavior matters; how they are aggregated into a spatio-temporal supervision mask is deferred to §4.2, which exploits the group structure of our RL algorithm. We instantiate  $\mathcal{M}_c$  in two stages: (i) offline specification synthesis which run once per task by a coding agent and frozen during RL; and (ii) per-rollout state lifting and clause evaluation.

**Specification synthesis.** Given the task context  $y = (c, \mathbf{I})$ , an offline coding agent synthesizes a triple  $(\mathcal{E}_c, \mathcal{P}_c, \Phi_c)$ : (i) a set of task-relevant entities  $\mathcal{E}_c$  (task-related robot and objects); (ii) an entity-grounded predicate library  $\mathcal{P}_c$  in which each predicate is already bound to concrete entities, e.g. GRASP(arm, cup) or IN(cup, drawer); and (iii) an LTL<sub>f</sub> conjunction  $\Phi_c = \bigwedge_{k=1}^K \varphi_k$  in which each clause  $\varphi_k$  is instantiated from a *closed template library* covering four families: *persistence*  $\mathbf{G} p$ , *terminal placement*  $\mathbf{FG} p$ , *causal coupling*  $\mathbf{G}(p \rightarrow q)$ , and *ordering*  $p \mathbf{U} q$ . The closed template library makes the next stage’s witness extraction template-driven rather than ad-hoc.

**State lifting and clause evaluation.** For each rollout  $x_0$ , we lift the video into a per-entity state trace  $\sigma(x_0; y) = (s_1, \dots, s_T)$  with  $s_t = \{s_t^e\}_{e \in \mathcal{E}_c}$ , where  $s_t^e$  collects the attributes of entity  $e$  at frame  $t$  (segmentation mask, 2D position, gripper open/close, attribute flags). Three vision foundation models cooperate on this lifting: SAM3 [5] for object masks and trajectories, IDM [14, 30] for robot and gripper states, and a VLM [31] for attribute checks such as whether a drawer is open. As a by-product, we collect each entity’s swept SAM3 mask  $m_e = \bigcup_t \text{SAM3}(e, t)$  across the trace into the atlas  $\mathcal{S} = \{m_e\}_{e \in \mathcal{E}_c}$ . Each predicate  $p \in \mathcal{P}_c$  is then evaluated as a Boolean stream  $b_p(t) = p(\sigma, t)$ , and each clause  $\varphi_k$  is evaluated by a finite-trace bottom-up monitor that returns a truth value  $r_k$  together with a violation witness  $W_k \subseteq \mathcal{E}_c \times [1, T]$  obtained by template-driven extraction (e.g.,  $\mathbf{G}(p \rightarrow q)$  produces  $W_k = \{(e, t) : b_p(t) \wedge \neg b_q(t)\}$ ,  $\mathbf{G} p$  produces the unsatisfied frames of  $b_p$ ); satisfied clauses contribute  $W_k = \emptyset$ . The rollout reward is the binary verdict  $r(x_0; y) = \mathbf{1}[\sigma \models \Phi_c] \in \{0, 1\}$ ; we pack the per-clause witnesses into  $\mathcal{V} = \{(k, W_k)\}_{k=1}^K$ , which together with  $\mathcal{S}$  is consumed by the credit-aware NFT loss in §4.2.

## 4.2 Credit-Aware NFT Loss

Video diffusion models update a high-dimensional pixel–frame tensor whose data manifold is low-dimensional [27, 29] and whose reward depends on only a small spatio-temporal region of that tensor [26, 18, 36]. Online RL is therefore prone to accumulate gradient error on coordinates outside this region, eventually causing off-manifold drift and policy collapse [33, 42]. Our binary reward makes things worse: an all-or-nothing gain governs the entire rollout, so reward-irrelevant pixels are pulled toward the positive or reflection target at the same strength as those carrying signal. We therefore restrict the residual of Eq. (4) to a spatio-temporal mask  $\mathbf{M}$ , aggregated from the per-rollout outputs of §4.1.

**Spatial-temporal credit mask.** We use a single  $\mathbf{M}$  shared across all  $N$  rollouts of a group rather than  $N$  per-sample masks, so that the positive and negative branches of the loss compete on a common support—successful rollouts are reinforced at exactly the coordinates where failed rollouts’ drift is penalized. Let  $\pi_t : \mathcal{E}_c \times [1, T] \rightarrow 2^{[1, T]}$  denote the projection of a witness set onto its frame indices. The temporal axis collects every frame implicated by any failing clause across the group, and the spatial axis unions the entity atlases of all rollouts:

$$\mathbf{M}_T = \bigcup_{i,k} \pi_t(W_k^{(i)}), \quad \mathbf{M}_S = \bigcup_{i,e} m_e^{(i)}, \quad \mathbf{M} = \mathbf{M}_T \otimes \mathbf{M}_S. \quad (6)$$

We treat  $\mathbf{M}_T \in \{0, 1\}^T$  and  $\mathbf{M}_S \in \{0, 1\}^{H \times W}$  as binary masks identified with their support sets, so  $\otimes$  produces a binary  $\mathbf{M} \in \{0, 1\}^{T \times H \times W}$ .  $\mathbf{M}_T$  contributions come only from failed clauses (satisfied

ones give  $W_k^{(i)} = \emptyset$ ), whereas  $\mathbf{M}_S$  unions all rollouts regardless of  $r^{(i)}$  to preserve the shared support. If the whole group succeeds,  $\mathbf{M}_T = \emptyset$  and  $\mathbf{M} \equiv 0$ , matching the vanishing group-relative advantage.

**Credit-aware NFT loss.** Gating both branches of Eq. (4) by  $\mathbf{M}$  yields

$$\mathcal{L}_{\text{NFT}}^{\text{CA}}(\theta) = \mathbb{E}_{i,t,\epsilon} \left[ r_i \|\mathbf{M} \odot (v_\theta^+ - v^{(i)})\|^2 + (1 - r_i) \|\mathbf{M} \odot (v_\theta^- - v^{(i)})\|^2 \right], \quad (7)$$

where  $\|\cdot\|^2$  is the element-wise sum of squares,  $\odot$  broadcasts along the channel dimension, and  $\mathbf{M} \equiv 1$  recovers Eq. (4) exactly. Analysis in Appendix A.2 shows that our credit-aware NFT loss preserves the improvement direction of the original NFT loss (Eq. (4)) while restricting updates to task-related pixels, thereby avoiding error accumulation on unrelated pixels—a substantial source of off-manifold drift in negative-aware finetuning [33, 42]. This design is critical on high-dimensional video: estimating the improvement direction jointly from a small rollout batch and the velocity anchor  $v_{\text{old}}$  is substantially noisy, and since reward depends on only a small spatio-temporal region of the pixel volume [26, 18, 36], our mask is essential to confine updates to that region and prevent the estimator noise from accumulating on the dominant task-irrelevant pixels.

### 4.3 Corrective Reflow Loss

Existing video RL post-training methods process each rollout in a group in isolation: every  $\mathbf{x}_0^{(i)}$  contributes only through its own residual paired with its scalar reward  $r_i$ , leaving the relational structure across the group unused [41, 37, 22, 20]. Our setting makes this structure unusually informative: under TI2V conditioning  $y = (c, \mathbf{I})$ , every within-group rollout starts from the same first frame, so the within-group successful rollouts are i.i.d. samples from the same condition-specific successful-rollout distribution, and their empirical mean is a pixel-level corrective continuation of any failed rollout exactly where the failure occurred. Instead of letting this relational signal act only implicitly, CrEFlow proposes a novel corrective reflow loss that explicitly supervises how each negative should be corrected on its failed regions, leading to faster and more stable post-training.

Let  $\mathcal{P} = \{i : r_i = 1\}$  and  $\mathcal{N} = \{i : r_i = 0\}$  denote the within-group positive and negative index sets. We use the empirical mean of the within-group positives as the corrective target:

$$\bar{\mathbf{x}}_0^+ := \frac{1}{|\mathcal{P}|} \sum_{j \in \mathcal{P}} \mathbf{x}_0^{(j)}. \quad (8)$$

Conditioned on  $y$ , the positives in  $\mathcal{P}$  are i.i.d. draws from the same successful-rollout distribution, so  $\bar{\mathbf{x}}_0^+$  is an unbiased estimator of the within-condition positive mean (App. A.3). Aggregating over the entire positive set also eliminates the matching-bias term that nearest-positive selection in any embedding would introduce.

**Loss form.** We reuse the group-shared mask  $\mathbf{M}$  of Eq. (6): its spatial support  $\mathbf{M}_S$  unions the entity atlases of both within-group positives and negatives, jointly bounding the failure-relevant support on the negatives and the corresponding corrective-content support on the positives—the dual support a substitution mask requires. Inverting the rectified-flow interpolation Eq. (2) gives the model’s one-step  $\mathbf{x}_0$ -prediction  $\hat{\mathbf{x}}_0^{(i)} := \mathbf{x}_t^{(i)} - t v_\theta(\mathbf{x}_t^{(i)}, t, y)$ . The corrective reflow loss regresses  $\hat{\mathbf{x}}_0^{(i)}$  toward  $\bar{\mathbf{x}}_0^+$  on  $\mathbf{M}$ , applied only to negatives:

$$\mathcal{L}_{\text{CR}}(\theta) = \mathbb{E}_{i \in \mathcal{N}, t, \epsilon} \left[ \|\mathbf{M} \odot (\hat{\mathbf{x}}_0^{(i)} - \bar{\mathbf{x}}_0^+)\|^2 \right]. \quad (9)$$

Analysis in Appendix A.5 shows that our corrective reflow loss stabilizes training with a strictly lower-variance *parameter-gradient* estimator: the within-group positive mean directly supplies the reward-induced improvement direction, eliminating the EMA-plug-in noise floor that NFT [41] incurs from reconstructing the same direction implicitly through the reflection of  $v_{\text{old}}$ .

**Overall training objective.** Combining the credit-aware NFT loss, the corrective reflow loss, and a KL regularizer to a frozen reference policy  $\pi_{\text{ref}}$  with parameters  $\theta_{\text{ref}}$  (the pretrained Vidar policy used to initialize post-training), the full CrEFlow objective reads

$$\mathcal{L}_{\text{CrEFlow}}(\theta) = \mathcal{L}_{\text{NFT}}^{\text{CA}}(\theta) + \lambda_{\text{CR}} \mathcal{L}_{\text{CR}}(\theta) + \lambda_{\text{KL}} \mathcal{L}_{\text{KL}}(\theta; \theta_{\text{ref}}), \quad (10)$$

where  $\lambda_{\text{CR}}, \lambda_{\text{KL}} > 0$  are scalar weights and  $\mathcal{L}_{\text{KL}}$  is the standard velocity-MSE KL surrogate to the reference policy.

## 5 Experiments

We design experiments to answer two questions: (Q1) does the compositional reward of §4.1 better reflect downstream manipulation success than existing video reward models, and does post-training under it yield higher real-task success? (Q2) does CreFlow optimize a sparse binary task reward more effectively than prior diffusion/flow RL algorithms? §5.1 fixes the protocol; §5.2 answers Q1+Q2 jointly via downstream task success and isolates Q1 on a held-out reward-fidelity set; §5.3 dissects CreFlow’s components.

### 5.1 Experimental Setup

**Tasks and base models.** We evaluate on eight RoboTwin [7] bimanual manipulation tasks covering pick-and-place, articulated manipulation, multi-object arrangement, and goal-conditioned placement. Following the video-as-policy pipeline of Vidar [14], we use the pretrained Vidar text-image-to-video model as the base VGM  $G_\theta$  and Vidar’s pretrained inverse dynamics model as the frozen action decoder  $\mathcal{I}$ ; only  $G_\theta$  is updated during post-training. The compositional constraint monitor of §4.1 is synthesized once per task with Claude Opus 4.6 and frozen.

**Baselines.** We compare against three groups. (i) *Policy-level reference*:  $\pi_{0.5}$  [4] and the un-post-trained Vidar base, reflecting the absolute scale of downstream success rather than competing with our post-training. (ii) *RL post-training*: DanceGRPO [37] and DiffusionNFT [41], applied to the same Vidar base under our binary reward with identical rollout budget and group size. (iii) *Reward baselines* (Tab. 2): EVA [34] (IDM-based continuous), WMReward [8] (JEPA-based continuous), VideoAlign [23] (appearance-based continuous), and a VLM-as-judge that prompts a frozen VLM (Gemini 3 Flash [31]) for a binary verdict on downsampled frames. The same Gemini 3 Flash checkpoint is used for the attribute-state predicate  $\text{STATE}(e, q)$  inside our monitor, so reward-fidelity comparisons against the VLM-as-judge baseline isolate the effect of LTL composition rather than VLM capability.

**Metrics.** For Q1+Q2 (§5.2, §5.3), we report *task success rate*: the fraction of episodes in which  $\mathcal{I}(\mathbf{x}_0)$ , executed in RoboTwin, completes the task; each cell averages 100 episodes per task. For Q1 reward fidelity (Tab. 2), we report agreement on a held-out 100-video set with two independent ground-truth labels (binary human and binary simulator-execution); see Tab. 2 caption for per-column definitions.

### 5.2 Main Results

**Benchmark comparison.** Tab. 1 compares CreFlow with policy-level references ( $\pi_{0.5}$ , Vidar base) and three video RL post-training baselines (EVA, DanceGRPO, DiffusionNFT) on all eight RoboTwin tasks. DanceGRPO, DiffusionNFT, and CreFlow share our binary compositional reward and differ only in optimizer; EVA bundles its own continuous IDM-based reward. We see that: i) CreFlow achieves the best success rate on every task, outperforming both VLA baseline ( $\pi_{0.5}$ ), video policy baseline (Vidar) and all video-RL post-training baselines, showing that our compositional reward and localized optimization strategy translate into consistent downstream execution gains. ii) EVA, the closest existing manipulation-video-RL baseline, improves only marginally over the Vidar base on average, suggesting that IDM-derived trajectory regularization alone is insufficient for evaluating contact-rich manipulation success. This is expected: penalizing low-level motion artifacts cannot verify whether a rollout satisfies the temporal and causal requirements of the task. iii) Under the same binary compositional reward, CreFlow substantially outperforms DanceGRPO and vanilla DiffusionNFT, indicating that the proposed credit-aware NFT and corrective reflow objectives are more effective for optimizing sparse video rewards than generic group-relative policy gradients or unlocalized negative-aware finetuning. iv) The gains are especially large on long-horizon, multi-stage tasks such as *put\_bottles\_dustbin* and *stack\_bowls\_three*, where success depends on satisfying a sequence of compositional constraints. This supports our design hypothesis: LTL-based verification provides faithful judgments for long-horizon rollouts, while violation traces allow CreFlow to focus updates on the reward-critical spatio-temporal regions.

**Training convergence.** Fig. 3 compares the post-training dynamics of DanceGRPO, DiffusionNFT, and CreFlow on three representative RoboTwin tasks: *rank\_blocks\_rgb*, *put\_bottles\_dustbin*, and *stack\_bowls\_three*. All methods start from the same Vidar base and optimize the same binary

Table 1: Downstream task success rate on eight RoboTwin manipulation tasks. Top block: policy-level references reflect absolute scale. Bottom block: video RL post-training methods, all built on the same Vidar base with the same rollout budget; DanceGRPO, DiffusionNFT, and CreFlow use our binary compositional reward, while EVA is a recent video-RL-for-robotic-manipulation method that uses its own continuous IDM-based reward.

Method	rank-blk	put-bot	put-cab	stk-bowl	stk-blk	dump-bin	open-lap	hand-mic	Avg.
$\pi_{0.5}$ [4]	25%	11%	33%	37%	9%	49%	46%	31%	30.1%
Vidar [14]	52%	3%	22%	39%	25%	42%	36%	24%	30.4%
EVA [34]	45%	5%	20%	44%	39%	56%	50%	15%	34.3%
DanceGRPO [37]	48%	5%	20%	38%	22%	41%	35%	26%	29.4%
DiffusionNFT [41]	52%	14%	36%	58%	41%	53%	49%	36%	42.4%
<b>CreFlow (Ours)</b>	<b>61%</b>	<b>24%</b>	<b>49%</b>	<b>75%</b>	<b>54%</b>	<b>61%</b>	<b>57%</b>	<b>44%</b>	<b>53.1%</b>

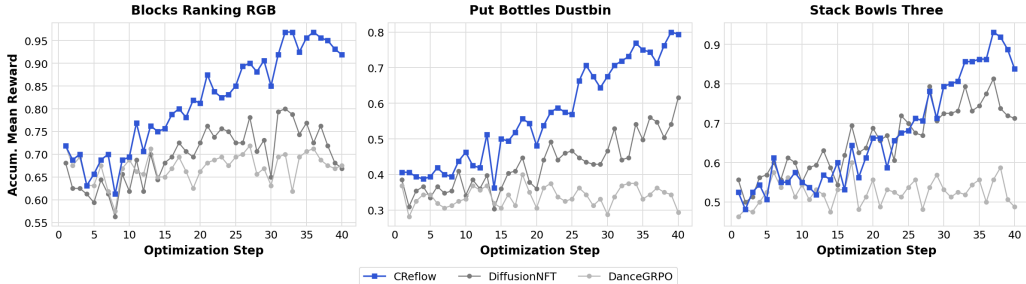


Figure 3: Training convergence on three RoboTwin tasks under the same binary compositional reward. Compared with DanceGRPO and DiffusionNFT, CreFlow converts sparse task feedback into faster and more stable reward improvement by localizing updates to violation-relevant frames and entities.

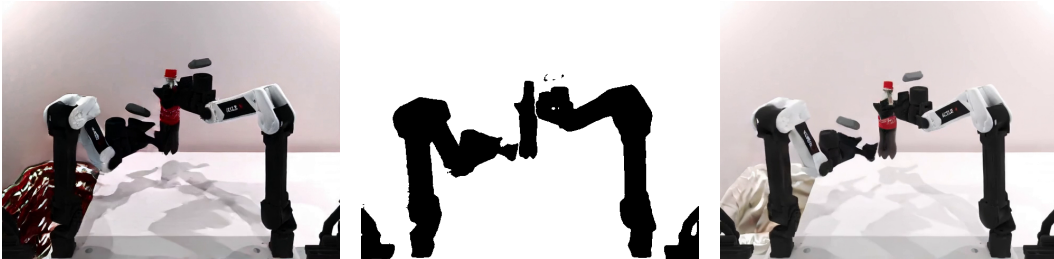
compositional reward, so the curves directly reflect how effectively each optimizer converts sparse task feedback into model improvement. We see that: i) CreFlow consistently rises faster and reaches the highest accumulated reward on all three tasks, indicating that localized correction improves not only final performance but also optimization efficiency. ii) DanceGRPO shows unstable or limited improvement: its SDE-style exploration and rollout-level policy-gradient update are not targeted to the sparse frames and entities that determine manipulation success, making the relative-advantage signal weak under binary rewards. iii) DiffusionNFT is more stable than DanceGRPO, but it plateaus at a lower reward because its negative-aware update is still applied over the full high-dimensional rollout without knowing which frames or entities caused failure.

**Reward fidelity to downstream success.** Tab. 2 compares our compositional reward with continuous video reward models and a VLM-as-judge baseline on 100 held-out videos, each labeled by both human judgment and simulator execution. We see that: i) CreFlow best matches downstream success, achieving 88.0% agreement with human labels and 91.0% with simulator labels. ii) Its pairwise ranking accuracy also reaches 0.893, clearly above the strongest continuous baseline EVA. iii) This gap suggests that global appearance, motion, or executability scores are insufficient proxies for manipulation success, which requires verifying a compositional task specification. iv) The VLM-as-judge baseline further shows that binary scoring alone is not enough; the advantage comes from LTL-based temporal verification over perception-grounded predicates.

**Computational overhead of the LTL monitor.** We profile the per-rollout cost of our reward pipeline on a single H100. A single rollout takes  $\sim 60$  s to sample, and one optimizer step on the LoRA-adapted backbone takes  $\sim 70$  s—both costs that any video-diffusion-RL method must already pay. On top of this, evaluating our compositional LTL reward on a generated video adds  $\sim 15$  s in total: SAM3 mask extraction is the dominant term ( $\sim 8$  s), the IDM gripper trace contributes  $\sim 1$  s, and the remainder is spent on LTL evaluation and VLM queries. Our reward computation therefore accounts for only a small fraction of the per-step wall-clock budget relative to rollout sampling and gradient update.

Table 2: Reward fidelity on 100 held-out evaluation videos with two independent ground-truth labels (human binary; simulator execution binary). Continuous rewards are reported with AUROC; binary rewards collapse AUROC to a single ROC point (marked “—”). Pairwise rank acc. is computed on all (success, failure) pairs under simulator labels.

Reward	Type	Acc. vs Human	F1 vs Human	Acc. vs Sim	AUROC vs Sim	Pairwise Rank Acc.
EVA [34]	Cont. (IDM)	74.0%	73.2%	78.0%	0.815	0.792
WMReward [8]	Cont. (JEPA)	70.0%	69.1%	73.0%	0.758	0.741
VideoAlign [23]	Cont. (Appearance)	63.0%	62.4%	65.0%	0.652	0.621
VLM-as-judge	Binary	71.0%	70.3%	74.0%	—	0.718
CreFlow (Ours)	<b>Binary</b>	<b>88.0%</b>	<b>87.4%</b>	<b>91.0%</b>	—	<b>0.893</b>



(a) Vanilla DiffusionNFT (no mask). (b) Group-shared mask  $M$ . (c) CreFlow (Ours).

Figure 4: Qualitative ablation on a *put\_bottles\_dustbin* rollout. (a) Vanilla DiffusionNFT, with no mask, visibly degrades the dustbin region during RL training. (b) Our group-shared mask  $M$  covers the task-relevant entities (arms, bottle); its complement is anchored to the pretrained prior. (c) CreFlow confines the contrastive update to  $M$ , preserving off-task visual quality.

### 5.3 Ablation Study

**Component ablation.** Tab. 3 dissects CreFlow into its two core mechanisms (the credit-aware NFT loss and the corrective reflow loss) on three representative tasks. We see that: i) credit-aware NFT alone (43.0% vs. 36.0%) closes most of vanilla NFT’s credit-assignment gap, confirming that the binary verdict depends on a small task-relevant subset of pixels and frames; ii) corrective reflow alone (39.0%) yields a smaller gain—without the violation-trace mask, the within-group positive prototype still drives gradient on off-task coordinates and dilutes the signal.

**Qualitative ablation.** Fig. 4 is the visual counterpart of the credit-aware-NFT-vs-vanilla row in Tab. 3: vanilla DiffusionNFT’s uniform contrastive update visibly degrades the dustbin region during RL training (Fig. 4a), even though those off-task pixels never enter the binary reward; restricting the update to  $M$  (Fig. 4b) anchors the rest of the scene to the pretrained prior and prevents this off-task collapse (Fig. 4c).

Table 3: Component ablation. Success rate (%) on three representative RoboTwin tasks.

Method	put-bot	stk-bowl	put-cab	Avg.
Vanilla DiffusionNFT	14%	58%	36%	36.0%
+ credit-aware NFT only	19%	67%	43%	43.0%
+ corrective reflow only	16%	62%	39%	39.0%
<b>+ both (Ours)</b>	<b>24%</b>	<b>75%</b>	<b>49%</b>	<b>49.3%</b>

## 6 Conclusion and Limitations

We propose CreFlow, a corrective reflow framework for post-training manipulation VGMs with sparse compositional rewards. CreFlow formulates task success as compositional LTL constraints and uses the resulting localized constraint violations to construct two targeted objectives: a credit-aware NFT loss that confines reward-induced updates to task-relevant regions, and a corrective reflow loss that uses same-condition successful rollouts as explicit correction targets for failed samples. Experiments show that CreFlow yields reward judgments better aligned with human and simulator success labels than existing methods, leads to effective training to improve high dimensional video generation, and improves downstream execution success by 23.8 percentage points. **Limitation and future work.** Our current monitor reasons over 2D image-plane states and therefore cannot fully resolve fine-grained 3D spatial relations. Extending the constraint evaluation with depth or 3D state estimation is a natural direction for future work.

## References

- [1] Niket Agarwal, Arslan Ali, Maciej Bala, Yogesh Balaji, et al. Cosmos world foundation model platform for physical AI. *arXiv preprint arXiv:2501.03575*, 2025.
- [2] Homanga Bharadhwaj, Debidatta Dwibedi, Abhinav Gupta, Shubham Tulsiani, Carl Doersch, Ted Xiao, Dhruv Shah, Fei Xia, Dorsa Sadigh, and Sean Kirmani. Gen2act: Human video generation in novel scenarios enables generalizable robot manipulation. *arXiv preprint arXiv:2409.16283*, 2024.
- [3] Hongzhe Bi, Hengkai Tan, Shenghao Xie, Zeyuan Wang, Shuhe Huang, Haitian Liu, Ruowen Zhao, Yao Feng, Chendong Xiang, Yinze Rong, et al. Motus: A unified latent action world model. *arXiv preprint arXiv:2512.13030*, 2025.
- [4] Kevin Black, Anthony Brohan, Danny Driess, Adnan Esmaeili, Chelsea Finn, Niccolo Fuentes, Brian Groom, Karol Hausman, Brian Ichter, Szymon Jakubczak, et al.  $\pi_{0.5}$ : a vision-language-action model with open-world generalization, 2025. *arXiv preprint arXiv:2504.16054*.
- [5] Nicolas Carion, Laura Gustafson, Yuan-Ting Hu, Shoubhik Debnath, Ronghang Hu, Didac Suris, Chaitanya Ryali, et al. SAM 3: Segment anything with concepts, 2025. *arXiv preprint arXiv:2511.16719*. Meta AI.
- [6] Boyuan Chen, Tianyuan Zhang, Haoran Geng, Kiwhan Song, Caiyi Zhang, Peihao Li, William T. Freeman, Jitendra Malik, Pieter Abbeel, Russ Tedrake, Vincent Sitzmann, and Yilun Du. Large video planner enables generalizable robot control. *arXiv preprint arXiv:2512.15840*, 2025.
- [7] Tianxing Chen, Zanxin Chen, Baijun Chen, Zijian Cai, Yibin Liu, Zixuan Li, Qiwei Liang, Xianliang Lin, Yiheng Ge, Zhenyu Gu, et al. RoboTwin 2.0: A scalable data generator and benchmark with strong domain randomization for robust bimanual robotic manipulation. *arXiv preprint arXiv:2506.18088*, 2025.
- [8] Yuzhi Chen, Ronghan Chen, Dongjie Huo, Yandan Yang, Dekang Qi, Haoyun Liu, Tong Lin, Shuang Zeng, Junjin Xiao, Xinyuan Chang, et al. ABot-PhysWorld: Interactive world foundation model for robotic manipulation with physics alignment. *arXiv preprint arXiv:2603.23376*, 2026.
- [9] Haoyuan Deng, Wenkai Guo, Qianzhun Wang, Zhenyu Wu, and Ziwei Wang. Safebimanual: Diffusion-based trajectory optimization for safe bimanual manipulation. *arXiv preprint arXiv:2508.18268*, 2025.
- [10] Karthik Dharmarajan, Wenlong Huang, Jiajun Wu, Li Fei-Fei, and Ruohan Zhang. Dream2Flow: Bridging video generation and open-world manipulation with 3D object flow. *arXiv preprint arXiv:2512.24766*, 2025.
- [11] Hongyang Du, Junjie Ye, Xiaoyan Cong, Runhao Li, Jingcheng Ni, Aman Agarwal, Zeqi Zhou, Zekun Li, Randall Balestriero, and Yue Wang. VideoGPA: Distilling geometry priors for 3D-consistent video generation. *arXiv preprint arXiv:2601.23286*, 2026.
- [12] Yilun Du, Mengjiao Yang, Bo Dai, Hanjun Dai, Ofir Nachum, Joshua B. Tenenbaum, Dale Schuurmans, and Pieter Abbeel. Learning universal policies via text-guided video generation. In *Advances in Neural Information Processing Systems (NeurIPS)*, 2023.
- [13] Yilun Du, Mengjiao Yang, Pete Florence, Fei Xia, Ayzaan Wahid, Brian Ichter, Pierre Sermanet, Tianhe Yu, Pieter Abbeel, Joshua B. Tenenbaum, Leslie Kaelbling, Andy Zeng, and Jonathan Tompson. Video language planning, 2023. *arXiv preprint arXiv:2310.10625*.
- [14] Yao Feng, Hengkai Tan, Xinyi Mao, Chendong Xiang, Guodong Liu, Shuhe Huang, Hang Su, and Jun Zhu. Vidar: Embodied video diffusion model for generalist manipulation. *arXiv preprint arXiv:2507.12898*, 2025.
- [15] Zirui Ge, Pengxiang Ding, Baohua Yin, Qishen Wang, Zhiyong Xie, Yemin Wang, Jinbo Wang, Hengtao Li, Runze Suo, Wenxuan Song, et al. VAMPO: Policy optimization for improving visual dynamics in video action models, 2026. *arXiv preprint arXiv:2603.19370*.

- [16] Yucheng Hu, Yanjiang Guo, Pengchao Wang, Xiaoyu Chen, Yen-Jen Wang, Jianke Zhang, Koushil Sreenath, Chaochao Lu, and Jianyu Chen. Video prediction policy: A generalist robot policy with predictive visual representations, 2024. *arXiv preprint arXiv:2412.14803*.
- [17] Wenlong Huang, Chen Wang, Yunzhu Li, Ruohan Zhang, and Li Fei-Fei. Rekep: Spatio-temporal reasoning of relational keypoint constraints for robotic manipulation. *arXiv preprint arXiv:2409.01652*, 2024.
- [18] Zitong Huang, Kaidong Zhang, Yukang Ding, Chao Gao, Rui Ding, Ying Chen, and Wangmeng Zuo. Mind the generative details: Direct localized detail preference optimization for video diffusion models, 2026. *arXiv preprint arXiv:2601.04068*.
- [19] Kimin Lee, Hao Liu, Moonkyung Ryu, Olivia Watkins, Yuqing Du, Craig Boutilier, Pieter Abbeel, Mohammad Ghavamzadeh, and Shixiang Shane Gu. Aligning text-to-image models using human feedback. *arXiv preprint arXiv:2302.12192*, 2023.
- [20] Junzhe Li, Yutao Cui, Tao Huang, Yiping Ma, Chun Fan, Miles Yang, Zhao Zhong, and Liefeng Bo. MixGRPO: Unlocking flow-based GRPO efficiency with mixed ODE-SDE, 2025. *arXiv preprint arXiv:2507.21802*.
- [21] Manling Li, Shiyu Zhao, Qineng Wang, Kangrui Wang, Yu Zhou, Sanjana Srivastava, Cem Gokmen, Tony Lee, Li E Li, Ruohan Zhang, et al. Embodied agent interface: Benchmarking llms for embodied decision making. *Advances in Neural Information Processing Systems*, 37: 100428–100534, 2024.
- [22] Jie Liu, Gongye Liu, Jiajun Liang, Yangguang Li, Jiaheng Liu, Xintao Wang, Pengfei Wan, Di Zhang, and Wanli Ouyang. Flow-GRPO: Training flow matching models via online RL, 2025. *arXiv preprint arXiv:2505.05470*.
- [23] Jie Liu, Gongye Liu, Jiajun Liang, Ziyang Yuan, Xiaokun Liu, Mingwu Zheng, Xiele Wu, Qiulin Wang, Menghan Xia, Xintao Wang, et al. Improving video generation with human feedback, 2025. *arXiv preprint arXiv:2501.13918*.
- [24] Teli Ma, Jia Zheng, Zifan Wang, Chunli Jiang, Andy Cui, Junwei Liang, and Shuo Yang. Dit4dit: Jointly modeling video dynamics and actions for generalizable robot control. *arXiv preprint arXiv:2603.10448*, 2026.
- [25] Yuhang Ma, Xiaoshi Wu, Keqiang Sun, and Hongsheng Li. Hpsv3: Towards wide-spectrum human preference score. In *Proceedings of the IEEE/CVF International Conference on Computer Vision*, pages 15086–15095, 2025.
- [26] Ziqi Ni et al. Seeing what matters: Visual preference policy optimization for visual generation, 2025. *arXiv preprint arXiv:2511.18719*.
- [27] Phillip Pope, Chen Zhu, Ahmed Abdelkader, Micah Goldblum, and Tom Goldstein. The intrinsic dimension of images and its impact on learning. In *International Conference on Learning Representations (ICLR)*, 2021. *arXiv preprint arXiv:2104.08894*.
- [28] Alec Radford, Jong Wook Kim, Chris Hallacy, Aditya Ramesh, Gabriel Goh, Sandhini Agarwal, Girish Sastry, Amanda Askell, Pamela Mishkin, Jack Clark, et al. Learning transferable visual models from natural language supervision. In *International conference on machine learning*, pages 8748–8763. PmLR, 2021.
- [29] Robin Rombach, Andreas Blattmann, Dominik Lorenz, Patrick Esser, and Björn Ommer. High-resolution image synthesis with latent diffusion models. In *IEEE/CVF Conference on Computer Vision and Pattern Recognition (CVPR)*, 2022. *arXiv preprint arXiv:2112.10752*.
- [30] Hengkai Tan, Yao Feng, Xinyi Mao, Shuhe Huang, Guodong Liu, Zhongkai Hao, Hang Su, and Jun Zhu. AnyPos: Automated task-agnostic actions for bimanual manipulation, 2025. *arXiv preprint arXiv:2507.12768*.
- [31] Gemini Team, Rohan Anil, Sebastian Borgeaud, Jean-Baptiste Alayrac, Jiahui Yu, Radu Soricut, Johan Schalkwyk, Andrew M Dai, Anja Hawth, Katie Millican, et al. Gemini: a family of highly capable multimodal models. *arXiv preprint arXiv:2312.11805*, 2023.

- [32] Jin Wang, Jianxiang Lu, Guangzheng Xu, Comi Chen, Haoyu Yang, Linqing Wang, Peng Chen, Mingtao Chen, Zhichao Hu, Longhuang Wu, et al. TAGRPO: Boosting GRPO on image-to-video generation with direct trajectory alignment, 2026. arXiv preprint arXiv:2601.05729.
- [33] Jing Wang, Jiajun Liang, Jie Liu, Henglin Liu, Gongye Liu, Jun Zheng, Wanyuan Pang, Ao Ma, Zhenyu Xie, Xintao Wang, Meng Wang, Pengfei Wan, and Xiaodan Liang. GRPO-Guard: Mitigating implicit over-optimization in flow matching via regulated clipping, 2025. arXiv preprint arXiv:2510.22319.
- [34] Ruixiang Wang, Qingming Liu, Yueci Deng, Guiliang Liu, Zhen Liu, and Kui Jia. EVA: Aligning video world models with executable robot actions via inverse dynamics rewards, 2026. arXiv preprint arXiv:2603.17808.
- [35] Zehan Wang, Tengfei Wang, Haiyu Zhang, Xuhui Zuo, Junta Wu, Haoyuan Wang, Wenqiang Sun, Zhenwei Wang, Chenjie Cao, Hengshuang Zhao, et al. WorldCompass: Reinforcement learning for long-horizon world models, 2026. arXiv preprint arXiv:2602.09022.
- [36] Ziyi Wu, Anil Kag, Ivan Skorokhodov, Willi Menapace, Ashkan Mirzaei, Igor Gilitschenski, Sergey Tulyakov, and Aliaksandr Siarohin. DenseDPO: Fine-grained temporal preference optimization for video diffusion models, 2025. arXiv preprint arXiv:2506.03517.
- [37] Zeyue Xue, Jie Wu, Yu Gao, Fangyuan Kong, Lingting Zhu, Mengzhao Chen, Zhiheng Liu, Wei Liu, Qiushan Guo, Weilin Huang, and Ping Luo. DanceGRPO: Unleashing GRPO on visual generation, 2025. arXiv preprint arXiv:2505.07818.
- [38] Seonghyeon Ye, Yunhao Ge, Kaiyuan Zheng, Shenyuan Gao, Sihyun Yu, George Kurian, Suneel Indupuru, You Liang Tan, Chuning Zhu, Jiannan Xiang, et al. World action models are zero-shot policies. *arXiv preprint arXiv:2602.15922*, 2026.
- [39] Simon Sinong Zhan, Yao Liu, Philip Wang, Zinan Wang, Qineng Wang, Yiyan Peng, Zhian Ruan, Xiangyu Shi, Xinyu Cao, Frank Yang, Kangrui Wang, Huajie Shao, Manling Li, and Qi Zhu. SENTINEL: A multi-level formal framework for safety evaluation of foundation model-based embodied agents. *arXiv preprint arXiv:2510.12985*, 2025.
- [40] Gehao Zhang, Zhenyang Ni, Payal Mohapatra, Han Liu, Ruohan Zhang, and Qi Zhu. EmboAlign: Aligning video generation with compositional constraints for zero-shot manipulation. *arXiv preprint arXiv:2603.05757*, 2026.
- [41] Kaiwen Zheng, Huayu Chen, Haotian Ye, Haoxiang Wang, Qinsheng Zhang, Kai Jiang, Hang Su, Stefano Ermon, Jun Zhu, and Ming-Yu Liu. DiffusionNFT: Online diffusion reinforcement with forward process, 2025. arXiv preprint arXiv:2509.16117.
- [42] Mingzhe Zheng, Weijie Kong, Yue Wu, Dengyang Jiang, Yue Ma, Xuanhua He, Bin Lin, Kaixiong Gong, Zhao Zhong, Liefeng Bo, et al. Manifold-aware exploration for reinforcement learning in video generation, 2026. arXiv preprint arXiv:2603.21872.
- [43] Enshen Zhou, Qi Su, Cheng Chi, Zhizheng Zhang, Zhongyuan Wang, Tiejun Huang, Lu Sheng, and He Wang. Code-as-monitor: Constraint-aware visual programming for reactive and proactive robotic failure detection. In *Proceedings of the Computer Vision and Pattern Recognition Conference*, pages 6919–6929, 2025.

## A Theoretical analysis of CreFlow

This appendix analyzes CreFlow as a *localized corrective stochastic estimator* for sparse-reward video diffusion RL. The two ingredients introduced in §4—violation-trace masking (§4.2) and the corrective reflow loss (§4.3)—are designed to fix two specific pathologies that arise when a sparse binary reward is fed into a flow-matching estimator on high-dimensional video. First, the reward signal is concentrated on a small failure-relevant region, but a vanilla negative-aware estimator spreads its gradient across the entire spatio-temporal volume, accumulating off-task residual noise on every step. Second, the only positive-side supervision available to the negative branch must be reconstructed from a reflected EMA plug-in, whose variance scales with the model’s own drift and is unrelated to the actual reward signal. CreFlow attacks both problems at the estimator level: violation masking projects the reward-induced learning signal onto the violation-traced coordinates and *exactly* cancels the off-mask sample noise that both branches structurally inject (§A.1–§A.2); the corrective branch replaces the reflected EMA plug-in with the within-group positive mean  $\bar{\mathbf{x}}_0^+$ , whose conditional first moment is the marginal positive prototype  $\mathbb{E}_{\pi^+(\cdot|y)}[x_0]$  (Lemma 1)—a  $t$ -uniform distributional anchor that coincides with the flow-matching positive velocity  $v^+(x_t, t)$  at high noise—and, when paired with the  $\mathbf{x}_0$ -space loss formulation’s automatic  $t^2$  down-weighting and the  $|\mathcal{P}|^{-1}$  within-group shrinkage, yields a strictly lower-variance *parameter-gradient* estimator at small  $t$  (§A.5).

We adopt DiffusionNFT [41] as the population reference for the *reward-induced improvement direction*  $\Delta = v^+ - v^{\text{old}}$ , since it gives a closed-form expression for the direction along which any positive-flow update should move the policy (§A.1, Theorem 1). CreFlow does not aim to reproduce the exact DiffusionNFT optimizer; rather, it remains positively aligned with  $\Delta$  on the active coordinates while improving the bias–variance tradeoff of the stochastic estimator. The three main results below formalize this contribution: Theorem 2 (§A.1) shows that violation-trace masking realizes a coordinate-localized estimator that retains the full  $\Delta$ -pull on the active support and imposes no constraint elsewhere; Proposition 1 (§A.4) shows that combining the two branches with a KL anchor yields an active-coordinate update positively aligned with  $\Delta$  on the violation mask, with a coordinate-dependent step length that combines the negative-aware contrastive pull and the corrective positive-mean pull; and Proposition 2 (§A.5) shows that, at the parameter-gradient level, the corrective branch (i) eliminates the persistent EMA reflection plug-in noise floor that the negative branch of NFT-style estimators carries by construction and (ii) leverages the  $\mathbf{x}_0$ -space loss formulation’s automatic  $t^2$  down-weighting (which converts the marginal-positive target’s  $\Theta(1/t^2)$  divergence into an  $O(t^2)$  vanishing gradient floor) and the  $|\mathcal{P}|^{-1}$  within-group averaging, yielding a strictly lower-variance gradient estimator at small  $t$ . §A.6 discusses the assumptions used along the way.

**Notation: trace-covariance.** Throughout this appendix, for a random vector  $X \in \mathbb{R}^d$  we use

$$\text{tr Cov}(X) := \sum_{k=1}^d \text{Var}(X_k) = \mathbb{E}\|X - \mathbb{E}X\|^2$$

as the scalar measure of target noise. Since all losses considered here are coordinate-wise squared errors in velocity or  $\hat{\mathbf{x}}_0$  prediction space, this quantity directly summarizes the amount of randomness seen by the least-squares estimator. We caution, however, that target trace-covariance and *parameter-gradient* trace-covariance need not move together: a loss formulated in  $\hat{\mathbf{x}}_0$ -space implicitly carries a  $t^2$  multiplicative factor on the velocity residual (Eq. (9)), which contributes a  $t^4$  multiplicative factor to the gradient covariance and can convert a  $\Theta(1/t^2)$ -divergent target covariance into an  $O(t^2)$  vanishing gradient floor (§A.5, Eqs. (44)–(46)). Variance-reduction claims in this appendix are therefore stated at the gradient level whenever the two diverge.

**Notation:  $v_\theta^{\text{old}}$  vs.  $v^{\text{old}}$ .** We follow the macro convention of §4:  $v^{\text{old}}(x_t, t)$  denotes the *population* conditional velocity field of the rollout distribution  $\pi^{\text{old}}$  (Eq. (12) below), while  $v_\theta^{\text{old}}(x_t, t)$  denotes the *EMA model’s* velocity prediction used as a plug-in estimator of  $v^{\text{old}}$ . The two coincide only in the noiseless limit; their difference  $\zeta_{\text{EMA}}$  is the source of the reflection plug-in noise analyzed in §A.5.

### A.1 Setup: reward-induced improvement direction

Fix the conditioning tuple  $c = (c_{\text{ext}}, c_{\text{img}})$  and suppress it from notation. Let  $\pi^{\text{old}}(x_0)$  be the rollout distribution induced by the current policy, and let  $r(x_0) \in \{0, 1\}$  be the binary reward. Define

$$p := \mathbb{E}_{x_0 \sim \pi^{\text{old}}}[r(x_0)], \quad \pi^+(x_0) := \frac{r(x_0)\pi^{\text{old}}(x_0)}{p}, \quad \pi^-(x_0) := \frac{(1-r(x_0))\pi^{\text{old}}(x_0)}{1-p}. \quad (11)$$

Under the rectified-flow forward convention

$$x_t = (1-t)x_0 + t\epsilon, \quad \epsilon \sim \mathcal{N}(0, I), \quad v = \epsilon - x_0 = \frac{x_t - x_0}{t},$$

let  $\pi_t^\bullet(x_t)$  be the time- $t$  marginal of  $\pi^\bullet$  for  $\bullet \in \{\text{old}, +, -\}$ . Define the conditional velocity field

$$v^\bullet(x_t, t) := \mathbb{E}_{x_0 \sim \pi^\bullet(\cdot | x_t, t)}[\epsilon - x_0 | x_t, t] = \frac{x_t - \mathbb{E}_{\pi^\bullet}[x_0 | x_t, t]}{t}. \quad (12)$$

The posterior mixture weight is

$$\alpha(x_t, t) := p \frac{\pi_t^+(x_t)}{\pi_t^{\text{old}}(x_t)}. \quad (13)$$

Bayes' rule gives the posterior split

$$\pi^{\text{old}}(x_0 | x_t, t) = \alpha(x_t, t)\pi^+(x_0 | x_t, t) + (1 - \alpha(x_t, t))\pi^-(x_0 | x_t, t), \quad (14)$$

and taking conditional expectations of  $v = \epsilon - x_0$  yields

$$v^{\text{old}} = \alpha v^+ + (1 - \alpha)v^-. \quad (15)$$

We define the positive-flow improvement direction

$$\Delta(x_t, t) := v^+(x_t, t) - v^{\text{old}}(x_t, t) = (1 - \alpha)(v^+ - v^-). \quad (16)$$

We recall the DiffusionNFT population optimizer in its  $\beta$ -parameterized form. For  $\beta > 0$ , DiffusionNFT uses

$$v_\theta^+ := (1 - \beta)v^{\text{old}} + \beta v_\theta, \quad v_\theta^- := (1 + \beta)v^{\text{old}} - \beta v_\theta,$$

and minimizes

$$\mathcal{L}_{\text{NFT}}^\beta(\theta) = \mathbb{E}_{t, \epsilon, x_0 \sim \pi^{\text{old}}}[r(x_0)\|v_\theta^+(x_t, t) - v\|^2 + (1 - r(x_0))\|v_\theta^-(x_t, t) - v\|^2]. \quad (17)$$

**Theorem 1** (DiffusionNFT population optimizer). *The pointwise minimizer of Eq. (17) satisfies*

$$v_{\theta^*}(x_t, t) = v^{\text{old}}(x_t, t) + \frac{2\alpha(x_t, t)}{\beta} \Delta(x_t, t). \quad (18)$$

*Proof.* Condition on  $(x_t, t)$  and differentiate Eq. (17) with respect to  $v_\theta$ . Since  $\nabla_{v_\theta} v_\theta^+ = \beta I$  and  $\nabla_{v_\theta} v_\theta^- = -\beta I$ , the first-order condition is

$$\mathbb{E}[r(x_0)(v_\theta^+ - v) | x_t, t] = \mathbb{E}[(1 - r(x_0))(v_\theta^- - v) | x_t, t]. \quad (19)$$

Using Eq. (14),

$$\mathbb{E}[r(x_0)f(x_0) | x_t, t] = \alpha(x_t, t)\mathbb{E}_{\pi^+}[f(x_0) | x_t, t],$$

and similarly  $\mathbb{E}[(1 - r(x_0))f(x_0) | x_t, t] = (1 - \alpha)\mathbb{E}_{\pi^-}[f(x_0) | x_t, t]$ . Thus Eq. (19) becomes

$$\alpha(v_\theta^+ - v^+) = (1 - \alpha)(v_\theta^- - v^-). \quad (20)$$

Let  $u := v_\theta - v^{\text{old}}$ . Then  $v_\theta^+ - v^+ = \beta u - \Delta$ , and by Eq. (15),  $v^- - v^{\text{old}} = -\frac{\alpha}{1-\alpha}\Delta$ , so  $v_\theta^- - v^- = -\beta u + \frac{\alpha}{1-\alpha}\Delta$ . Substituting into Eq. (20) gives

$$\alpha(\beta u - \Delta) = (1 - \alpha)\left(-\beta u + \frac{\alpha}{1-\alpha}\Delta\right),$$

which simplifies to  $\beta u = 2\alpha\Delta$ , i.e.  $v_{\theta^*} = v^{\text{old}} + (2\alpha/\beta)\Delta$ .  $\square$

**Assumption 1** (Population-level mask). *In the population analysis of the credit-aware NFT loss in Eq. (7) and the corrective reflow loss in Eq. (9), we treat the group-shared mask  $\mathbf{M} \in \{0, 1\}^D$  as a deterministic projection at the population level—equivalently, as  $\sigma(x_t, t)$ -measurable—so that  $\mathbf{M}(\omega)$  can be factored out of  $\mathbb{E}[\cdot | x_t, t]$ . The empirical  $\mathbf{M}$  in Eq. (6) is computed from the within-group un-noised rollouts  $\{\mathbf{x}_0^{(j)}\}_{j=1}^N$  (via the LTL violation traces  $\{W_k^{(j)}\}$  and the SAM3 atlases  $\{m^{(j), \epsilon}\}$ ); the assumption asserts that, at the population level, this empirical  $\mathbf{M}$  collapses to the reward-locality support depending only on  $(x_t, t)$  that underlies Eq. (22). See §A.6 for discussion.*

**Theorem 2** (Violation-localized pointwise optimum). *Under Assumption 1, for the credit-aware NFT loss in Eq. (7) with mask  $\mathbf{M} \in \{0, 1\}^D$ , the pointwise minimizer satisfies*

$$\mathbf{M} \odot (v_{\theta^*}(x_t, t) - v^{\text{old}}(x_t, t)) = \mathbf{M} \odot \frac{2\alpha(x_t, t)}{\beta} \Delta(x_t, t), \quad (21)$$

with  $\alpha$  and  $\Delta = v^+ - v^{\text{old}}$  as in Theorem 1. At coordinates with  $\mathbf{M}(\omega) = 0$  the masked loss is constant in  $v_{\theta}(\omega)$  and imposes no constraint.

*Proof.* At each  $(x_t, t, \omega)$  the squared-error coordinate-wise gradient contains a factor  $\mathbf{M}(\omega)^2 \geq 0$ . By Assumption 1,  $\mathbf{M}(\omega)$  is  $\sigma(x_t, t)$ -measurable and can be factored out of the conditional expectation  $\mathbb{E}[\cdot | x_t, t]$ , so the first-order condition at  $(x_t, t, \omega)$  is

$$\mathbf{M}(\omega)^2 \left( \mathbb{E}[r(x_0)(v_{\theta^+}(\omega) - v(\omega)) | x_t, t] - \mathbb{E}[(1 - r(x_0))(v_{\theta^-}(\omega) - v(\omega)) | x_t, t] \right) = 0.$$

At  $\mathbf{M}(\omega) = 0$  it is satisfied for any  $v_{\theta}(\omega)$ ; at  $\mathbf{M}(\omega) = 1$  it reduces to the unmasked first-order condition Eq. (19), whose unique solution is given by Theorem 1.  $\square$

**Pixel-wise improvement strength.** Eq. (21) shows that the violation-localized estimator concentrates its update strength on the failure-relevant coordinates: it retains the full  $2\alpha/\beta$  pull along the reward-induced direction  $\Delta$  on  $\mathbf{M}$  and zeros it elsewhere, in contrast to the coordinate-uniform pull of vanilla negative-aware finetuning [41]. The variance grounds for why this localization is desirable on high-dimensional video are deferred to the branch decomposition of §A.2.

**Step length.** For the unmasked reference estimator, Theorem 1 pulls  $v_{\theta}$  toward  $v^{\text{old}} + (2\alpha(x_t, t)/\beta) \Delta(x_t, t)$  at every coordinate<sup>1</sup>; CreFlow’s violation-localized estimator (Theorem 2) restricts this pull to the active coordinates of  $\mathbf{M}$  and leaves off-mask coordinates unconstrained. The analysis below studies how the corrective loss further shapes this estimator and how masking affects its gradient variance.

## A.2 Branch-level decomposition of off-mask noise

Theorem 2 gates the per-coordinate NFT step to zero outside  $\mathbf{M}$ . We give the intuition for why this is desirable on high-dimensional video by tracing the unmasked NFT residual back to its two reward-conditional branches, then state the off-mask reward-locality property that makes the masked estimator unbiased.

**Positive branch** ( $r_i = 1$ ). This branch reduces to a rejection-style flow-matching update [19, 41] that regresses  $v_{\theta^+}$  toward the rollout’s own velocity  $v^{(i)} = (x_t - x_0^{(i)})/t$ . Even on a successful rollout,  $v^{(i)}$  matches the population positive velocity  $v^+$  only on coordinates where the reward signal actually distinguishes  $\pi^+$  from  $\pi^{\text{old}}$ ; on task-irrelevant coordinates the rollout’s pixel-level content is one stochastic draw whose value is dominated by background, lighting, and rendering variation. The rejection-FT update injects this rollout-specific irrelevant variation into  $v_{\theta}$  on every off-mask pixel.

**Negative branch** ( $r_i = 0$ ). This branch trains  $v_{\theta^-} = (1 + \beta)v^{\text{old}} - \beta v_{\theta}$  toward  $v^{(i)}$ , equivalently pulling  $v_{\theta}$  toward the reflection target  $v_f^{(i)} = v^{\text{old}} + \frac{1}{\beta}(v^{\text{old}} - v^{(i)})$  centered on  $v^{\text{old}}$ . NFT’s design relies on the population identity  $v^{\text{old}} = \alpha v^+ + (1 - \alpha)v^-$  (Eq. (15)): on coordinates where  $\pi^+ = \pi^-$

<sup>1</sup>The prefactor  $2\alpha/\beta$  combines the reinforcement-guidance strength  $2/\beta$  with the posterior-positive weight  $\alpha(x_t, t)$ : at regions of the latent space where the current policy has high positive mass ( $\alpha \rightarrow 1$ ) the model takes a full  $(2/\beta)\Delta$  step, and where positive mass is low ( $\alpha \rightarrow 0$ ) it barely moves, consistent with the posterior weighting. In the limit  $\beta \rightarrow 0$  one recovers vanilla diffusion supervised fitting with an infinitely amplified  $\alpha\Delta$  step, which is exactly the regime that benefits most from variance reduction.

(off-mask under reward locality),  $v^+$  and  $v^-$  both collapse to  $v^{\text{old}}$ , so the conditional expectation of the reflection target equals  $v^{\text{old}}$  exactly—in expectation the reflection trick correctly leaves task-irrelevant content unchanged. The empirical reflection from a single rollout, however, retains the full conditional variance of  $v^{(i)}$  on every coordinate; off-mask, that variance is the inherent dispersion of  $\pi^{\text{old}}$ -conditional pixel content (background, lighting, rendering), and the negative-branch update trains  $v_\theta$  on this noise rather than on the intended reflection axis.

**Net effect.** Both branches therefore inject coordinate-wise residual noise on coordinates where the population improvement direction  $\Delta = v^+ - v^{\text{old}}$  vanishes. The formal off-mask reward-locality statement is: with  $\mathbf{P} = \text{Diag}(\mathbf{M})$ ,

$$(I - \mathbf{P})v^+(x_t, t) = (I - \mathbf{P})v^-(x_t, t) = (I - \mathbf{P})v^{\text{old}}(x_t, t), \quad (22)$$

which is the intended behavior of the monitor-derived mask of §4.1:  $\mathbf{P}$  is the union of every per-rollout violation pattern in the group, so coordinates outside it carry no clause-level disagreement on any rollout. By Theorem 2 the masked update is supported entirely on  $\mathbf{M}$ , so under Eq. (22) the masked estimator removes both branches’ off-mask sample noise without biasing the population update; without the mask, the same noise is treated as an improvement direction on every pixel and accumulates across gradient steps.

**Off-mask second-moment decomposition.** The branch-level intuition above admits a closed-form quantification at the population level. Set  $\bar{\mathbf{P}} := I - \mathbf{P}$  and probe the residual at  $v_\theta = v^{\text{old}}$ , so the active-coordinate  $\Delta$ -correction is realized on  $\mathbf{M}$  and the off-mask residual is read off the data side alone. Treating the reflection axis  $v^{\text{old}}$  as the population conditional velocity (deferring the EMA plug-in version  $v_\theta^{\text{old}}$  to §A.5), the conditional second moments of the two branches’ off-mask residuals factor as

$$\mathbb{E} \left[ r_i \|\bar{\mathbf{P}}(v_\theta^+ - v^{(i)})\|^2 \mid x_t, t \right] = \alpha(x_t, t) \text{tr Cov}_{\pi^+}[\bar{\mathbf{P}}v \mid x_t, t], \quad (23)$$

$$\mathbb{E} \left[ (1 - r_i) \|\bar{\mathbf{P}}(v_\theta^- - v^{(i)})\|^2 \mid x_t, t \right] = (1 - \alpha(x_t, t)) \text{tr Cov}_{\pi^-}[\bar{\mathbf{P}}v \mid x_t, t], \quad (24)$$

where  $v = \epsilon - x_0$  and the off-mask bias terms  $\bar{\mathbf{P}}(v^{\text{old}} - v^\pm)$  vanish by reward locality (Eq. (22)). Each line is the conditional pixel dispersion of the corresponding branch’s  $x_0$  distribution: rollout-specific background, lighting, and rendering variation which, under reward locality, coincides off-mask with the dispersion of  $\pi^{\text{old}} \mid (x_t, t)$  and is therefore reward-irrelevant. Theorem 2 zeroes the entire  $\bar{\mathbf{P}}$ -row of the masked loss at the population level, so the masked estimator eliminates both contributions exactly while leaving the  $\mathbf{P}$ -row residual—the only one supporting  $\Delta$ -aligned signal—intact. The implemented loss replaces  $v^{\text{old}}$  in  $v_\theta^\pm$  by an EMA plug-in  $v_\theta^{\text{old}}$ , which adds a separate reflection-axis noise term that concentrates on the negative branch at the paper’s setting  $\beta = 1$ ; this additional source is orthogonal to the masking story analyzed here and is taken up in §A.5 as the motivation for the corrective reflow loss of §4.3.

### A.3 Masks and local quadratic form

For a rollout group under the same conditioning, let  $\mathcal{N} := \{i : r_i = 0\}$  and  $\mathcal{P} := \{i : r_i = 1\}$  (consistent with §4.3), and let  $\bar{\mathbf{x}}_0^+ := |\mathcal{P}|^{-1} \sum_{j \in \mathcal{P}} \mathbf{x}_0^{(j)}$  denote the within-group positive mean of Eq. (8).

The credit-aware NFT and corrective reflow branches share the same group-shared violation-trace mask:

$$\mathbf{P} := \text{Diag}(\mathbf{M}), \quad (25)$$

which is a function of the entire group’s outputs and is not indexed by  $i$ .

**Marginal-prototype consistency of the positive mean.** The within-group positives  $\{\mathbf{x}_0^{(j)}\}_{j \in \mathcal{P}}$  are i.i.d. draws from  $\pi^+(\cdot \mid y)$ , sampled *independently* of the negative rollout  $i$  given  $y$ . In particular,  $\bar{\mathbf{x}}_0^+ \perp x_t^{(i)} \mid y$ , so

$$\mathbb{E}[\bar{\mathbf{x}}_0^+ \mid x_t, t] = \mathbb{E}[\bar{\mathbf{x}}_0^+ \mid y] = \mathbb{E}_{x_0 \sim \pi^+(\cdot \mid y)}[x_0], \quad (26)$$

i.e. the corrective target is an unbiased estimator of the *marginal* positive mean (a positive-prototype constant in  $x_t$ ), not of the flow-matching conditional positive mean  $\mathbb{E}_{\pi^+}[x_0 \mid x_t, t]$ . Conceptually, this is a deliberate choice: the corrective loss provides a  $t$ -uniform distributional anchor that pulls the

model’s  $\hat{x}_0$  prediction toward  $\pi^+$ ’s marginal content on the violation mask, while the credit-aware NFT branch supplies the  $t$ -dependent flow-matching pull. The two regimes coincide at high noise ( $t \rightarrow 1$ , where  $x_t$  is uninformative about  $x_0$  and conditional collapses to marginal) and complement each other at low noise. The within-step covariance of  $\hat{\mathbf{x}}_0^+$  shrinks by a factor of  $|\mathcal{P}|^{-1}$  relative to any single within-group positive, which yields the variance reduction analyzed in §A.5.

**Local quadratic KL approximation.** We use the following local approximation for the KL regularizer:

$$\mathcal{L}_{\text{KL}}(\theta; \theta_{\text{ref}}) \doteq \gamma_i \|v_\theta - v_{\text{ref}}\|^2, \quad \gamma_i \geq 0, \quad (27)$$

where  $v_{\text{ref}} := v_{\theta_{\text{ref}}}$  denotes the velocity field of the frozen reference policy  $\pi_{\text{ref}}$  and  $\gamma_i \geq 0$  is the local stiffness coefficient; this is the standard local quadratic approximation of the KL around the current iterate. Importantly, unless  $v_{\text{ref}} = v^{\text{old}}$  and the KL is isotropic in the local velocity coordinates, the KL term can move the optimum and can also rotate the update direction.

#### A.4 Coordinate-wise improvement alignment

We first record the velocity-space interpretation of the corrective loss. The corrective reflow loss is written in  $\hat{\mathbf{x}}_0$ -prediction space:

$$\hat{\mathbf{x}}_0^{(i)} = x_t^{(i)} - t v_\theta(x_t^{(i)}, t), \quad \mathcal{L}_{\text{CR}}^{(i)} = \lambda_{\text{CR}} \|\mathbf{P}(\hat{\mathbf{x}}_0^{(i)} - \bar{\mathbf{x}}_0^+)\|^2.$$

This is exactly equivalent to a velocity-space regression

$$\mathcal{L}_{\text{CR}}^{(i)} = \lambda_{\text{CR}} t^2 \|\mathbf{P}(v_\theta(x_t^{(i)}, t) - \tilde{v}_i^*)\|^2, \quad \tilde{v}_i^* := \frac{x_t^{(i)} - \bar{\mathbf{x}}_0^+}{t}. \quad (28)$$

Thus the corrective-reflow velocity target is  $\tilde{v}_i^* = (x_t^{(i)} - \bar{\mathbf{x}}_0^+)/t$ .

**Lemma 1** (Population target of the corrective loss). *Under Assumption 1, conditioned on  $(x_t, t)$ , the population target of the corrective branch is the marginal positive-prototype velocity restricted to the violation mask:*

$$\mathbf{P} \mathbb{E}[\tilde{v}_i^* | x_t, t] = \frac{1}{t} \mathbf{P}(x_t - \mathbb{E}_{\pi^+(\cdot|y)}[x_0]) =: \mathbf{P} \bar{v}^+(x_t, t). \quad (29)$$

*The right-hand side coincides with the flow-matching positive velocity  $\mathbf{P} v^+(x_t, t)$  at high noise ( $t \rightarrow 1$ , where the  $x_t$ -conditional and the  $y$ -conditional positive means agree); at finite  $t$  the two differ by the conditional positive entropy under the flow-matching joint.*

*Proof.* By Eq. (28) and Assumption 1 (which lets  $\mathbf{P} = \text{Diag}(\mathbf{M})$  be factored out of  $\mathbb{E}[\cdot | x_t, t]$ ),

$$\mathbf{P} \mathbb{E}[\tilde{v}_i^* | x_t, t] = \frac{1}{t} \mathbf{P}(x_t - \mathbb{E}[\bar{\mathbf{x}}_0^+ | x_t, t]).$$

The within-group positives  $\{\mathbf{x}_0^{(j)}\}_{j \in \mathcal{P}}$  are i.i.d. from  $\pi^+(\cdot | y)$ , sampled independently of  $x_t^{(i)}$  given  $y$ , so  $\mathbb{E}[\bar{\mathbf{x}}_0^+ | x_t, t] = \mathbb{E}_{\pi^+(\cdot|y)}[x_0]$  by Eq. (26), which gives the equality. At  $t = 1$ ,  $x_t = \epsilon$  is uninformative about  $x_0$  under the flow-matching joint as well, so  $\mathbb{E}_{\pi^+}[x_0 | x_t, t] = \mathbb{E}_{\pi^+(\cdot|y)}[x_0]$ , and  $\bar{v}^+ = v^+$  at the boundary.  $\square$

We can now write the local pointwise objective for a negative sample  $i$ . Define the marginal-prototype direction

$$\bar{\Delta}(x_t, t) := \bar{v}^+(x_t, t) - v^{\text{old}}(x_t, t) = \Delta(x_t, t) + \frac{1}{t} (\mathbb{E}_{\pi^+}[x_0 | x_t, t] - \mathbb{E}_{\pi^+(\cdot|y)}[x_0]), \quad (30)$$

so that  $\bar{\Delta} = \Delta$  at  $t = 1$  and the residual  $\bar{\Delta} - \Delta$  is the conditional-vs-marginal posterior gap of  $\pi^+$  at  $(x_t, t)$ . Let

$$\mu_{\text{NFT}} := v^{\text{old}} + \frac{2\alpha}{\beta} \Delta, \quad \mu_{\text{CR}} := \bar{v}^+ = v^{\text{old}} + \bar{\Delta}. \quad (31)$$

Let  $a_i > 0$  denote the local weight of the credit-aware NFT squared residual, and let  $b_i = \lambda_{\text{CR}} t^2$  denote the local weight of the corrective-reflow squared residual. The local quadratic approximation is

$$Q_i(v) = a_i \|\mathbf{P}(v - \mu_{\text{NFT}})\|^2 + b_i \|\mathbf{P}(v - \mu_{\text{CR}})\|^2 + \gamma_i \|v - v_{\text{ref}}\|^2. \quad (32)$$

**Proposition 1** (Active-coordinate update of CreFlow). *Assume either  $\gamma_i > 0$ , or that the support is restricted to active coordinates so that  $(a_i + b_i)\mathbf{P}$  is invertible on the active subspace  $\mathbf{P}$ . The pointwise minimizer of Eq. (32) is*

$$v_i^* = ((a_i + b_i)\mathbf{P} + \gamma_i I)^{-1} \left[ a_i \mathbf{P} (v^{\text{old}} + \frac{2\alpha}{\beta} \Delta) + b_i \mathbf{P} (v^{\text{old}} + \bar{\Delta}) + \gamma_i v_{\text{ref}} \right]. \quad (33)$$

If  $v_{\text{ref}} = v^{\text{old}}$ , then on  $\mathbf{P}$

$$\begin{aligned} v_i^* - v^{\text{old}} &= D_i^{\text{NFT}} \Delta + D_i^{\text{CR}} \bar{\Delta}, \\ D_i^{\text{NFT}} &:= ((a_i + b_i)\mathbf{P} + \gamma_i I)^{-1} \left( \frac{2\alpha a_i}{\beta} \right) \mathbf{P}, \\ D_i^{\text{CR}} &:= ((a_i + b_i)\mathbf{P} + \gamma_i I)^{-1} b_i \mathbf{P}. \end{aligned} \quad (34)$$

The NFT branch contributes a  $\Delta$ -aligned pull on  $\mathbf{P}$ ; the corrective branch contributes a  $\bar{\Delta}$ -aligned marginal-prototype pull on  $\mathbf{P}$ . The two pulls coincide at high noise ( $t \rightarrow 1$ , where  $\bar{\Delta} = \Delta$ ) and, at finite  $t$ , jointly drive a positive-side correction whose deviation from a pure  $\Delta$  ray is bounded by  $b_i \|\bar{\Delta} - \Delta\|$ .

*Proof.* The objective in Eq. (32) is a positive weighted sum of diagonal quadratic forms. Its first-order condition is

$$a_i \mathbf{P} (v - \mu_{\text{NFT}}) + b_i \mathbf{P} (v - \mu_{\text{CR}}) + \gamma_i (v - v_{\text{ref}}) = 0.$$

Solving this linear system gives Eq. (33). Well-posedness of the inverse follows from the assumption: when  $\gamma_i > 0$  the matrix is strictly positive definite; otherwise, on the active subspace  $\mathbf{P}$ ,  $(a_i + b_i)\mathbf{P}$  is positive definite there. If  $v_{\text{ref}} = v^{\text{old}}$ , subtract  $v^{\text{old}}$  from both sides, use  $\mu_{\text{NFT}} - v^{\text{old}} = \frac{2\alpha}{\beta} \Delta$  and  $\mu_{\text{CR}} - v^{\text{old}} = \bar{\Delta}$ , and split the result along the two directions to obtain Eq. (34).  $\square$

**Interpretation.** CreFlow’s active-coordinate update on  $\mathbf{P}$  is a superposition of two positively oriented pulls: an NFT contribution along the reward-induced direction  $\Delta$ , and a corrective contribution along the marginal-prototype direction  $\bar{\Delta}$ . The violation-traced mask  $\mathbf{P}$  identifies the support on which both pulls are applied; Eq. (34) factors them through the diagonal weights  $D_i^{\text{NFT}}$  and  $D_i^{\text{CR}}$ . Outside  $\mathbf{P}$  the update is anchored to the prior. The NFT and corrective directions agree at high noise and differ only by the conditional-vs-marginal posterior gap of  $\pi^+$  at finite  $t$ ; the corrective branch therefore complements rather than competes with the NFT pull, replacing a noisy reflection-EMA step with a low-variance marginal-prototype step that preserves the macroscopic structure of  $\Delta$ .

## A.5 EMA-free corrective branch and gradient variance

We now show that CreFlow’s corrective branch yields a strictly lower-variance *parameter-gradient estimator* than the NFT branch at small noise levels, even though its raw velocity target has a  $\Theta(1/t^2)$ -divergent per-step covariance. The reduction at the gradient level arises from two unconditional mechanisms: (i) the corrective branch is structurally EMA-free (no reflected  $v_\theta^{\text{old}}$  noise floor), and (ii) the  $\mathbf{x}_0$ -space loss formulation (Eq. (9)) injects a  $t^2$  down-weighting of the gradient, which exactly cancels the  $\Theta(1/t^2)$  target divergence and leaves an  $O(t^2)$  vanishing residual. Throughout this subsection we use the convention that  $v_\theta^{\text{old}}(x_t, t)$  denotes the EMA model’s velocity prediction (a plug-in estimator of  $v^{\text{old}}$ ), while  $v^{\text{old}}(x_t, t)$  denotes the true population conditional velocity; the two coincide only in the noiseless limit.

For a negative sample, the NFT reflected target induced by  $v_\theta^- = (1 + \beta)v_\theta^{\text{old}} - \beta v_\theta$  (the per-sample analogue of  $v_f^{(i)}$  in §A.2) is

$$\begin{aligned} Z_{\text{NFT}}^{(i)} &:= v_\theta^{\text{old}}(x_t^{(i)}, t) + \frac{1}{\beta} (v_\theta^{\text{old}}(x_t^{(i)}, t) - v^{(i)}) = \frac{\beta+1}{\beta} v_\theta^{\text{old}}(x_t^{(i)}, t) - \frac{1}{\beta} v^{(i)}, \\ v^{(i)} &= \epsilon - \mathbf{x}_0^{(i)} = \frac{x_t^{(i)} - \mathbf{x}_0^{(i)}}{t}. \end{aligned} \quad (35)$$

The corrective target induced by the actual corrective reflow loss is

$$Z_{\text{CR}}^{(i)} := \tilde{v}_i^* = \frac{x_t^{(i)} - \bar{\mathbf{x}}_0^+}{t}. \quad (36)$$

Unlike  $Z_{\text{NFT}}^{(i)}$ , the corrective-reflow target neither uses the EMA reflection axis  $v_\theta^{\text{old}}$  nor depends on a single stochastic positive draw.

**Within-step variance from a single positive.** For comparison, consider a hypothetical single-positive variant of the corrective branch in which the target is  $Z_{\text{CR},\text{single}}^{(i,j)} := (x_t^{(i)} - \mathbf{x}_0^{(j)})/t$  for one fixed  $j \in \mathcal{P}$ . Conditional on  $(x_t^{(i)}, x_0^{(i)})$ , and using  $\mathbf{x}_0^{(j)} \perp x_t^{(i)} \mid y$  (Lemma 1),

$$\text{Cov} \left[ \mathbf{P} Z_{\text{CR},\text{single}}^{(i,j)} \mid x_t^{(i)}, x_0^{(i)} \right] = \frac{1}{t^2} \text{Cov}_{\pi+(\cdot|y)}[\mathbf{P} x_0]. \quad (37)$$

With the within-group positive mean  $\bar{\mathbf{x}}_0^+$ , by independence of the  $|\mathcal{P}|$  positives,

$$\text{Cov} \left[ \mathbf{P} Z_{\text{CR}}^{(i)} \mid x_t^{(i)}, x_0^{(i)} \right] = \frac{1}{|\mathcal{P}|t^2} \text{Cov}_{\pi+(\cdot|y)}[\mathbf{P} x_0], \quad (38)$$

i.e. aggregating over  $|\mathcal{P}|$  within-group positives shrinks the within-step target covariance of the corrective branch by exactly the factor  $|\mathcal{P}|^{-1}$  relative to any single-positive variant, without changing its first moment (Lemma 1). We deliberately use the *marginal* covariance  $\text{Cov}_{\pi+(\cdot|y)}[\mathbf{P} x_0]$  on the right-hand side rather than a flow-matching posterior covariance  $\text{Cov}_{\pi+}[\mathbf{P} x_0 \mid x_t, t]$ : because  $\bar{\mathbf{x}}_0^+ \perp x_t^{(i)} \mid y$ , conditioning on  $x_t^{(i)}$  provides no additional information about the positives, and the conditional covariance collapses to the within-condition marginal, which is  $t$ -independent. The corrective target’s per-step covariance therefore genuinely diverges as  $\Theta(1/t^2)$  at small  $t$ , rather than vanishing as a flow-matching posterior would suggest.

**Across-history plug-in variance.** If we additionally analyze variability across training histories, the EMA buffer is a random plug-in estimator. Write

$$v_\theta^{\text{old}}(x_t, t) = v^{\text{old}}(x_t, t) + \xi_{\text{EMA}}(x_t, t), \quad \mathbb{E}[\xi_{\text{EMA}}] = 0, \quad (39)$$

and assume  $\xi_{\text{EMA}}$  is independent of the fresh current rollout conditional on  $(x_t, t)$ . Then for any fixed projector  $A$ ,

$$\text{Cov} \left[ A Z_{\text{NFT}}^{(i)} \mid x_t, t \right] = \frac{1}{\beta^2} \text{Cov} \left[ A v^{(i)} \mid x_t, t \right] + \frac{(\beta+1)^2}{\beta^2} \text{Cov} \left[ A \xi_{\text{EMA}}(x_t, t) \right]. \quad (40)$$

The coefficients  $1/\beta^2$  and  $(\beta+1)^2/\beta^2$  are the squared coefficients of  $v^{(i)}$  and  $v_\theta^{\text{old}}$  in the reflection target Eq. (35). The corrective target  $Z_{\text{CR}}^{(i)}$  contributes no EMA-plug-in term to its covariance.

**Parameter-gradient covariance and Jacobian alignment.** Let  $J(x_t, t, y) := \partial v_\theta(x_t, t, y)/\partial \theta$  denote the velocity-field Jacobian with respect to the trainable parameters, and write  $K := J J^\top$  for its Gram matrix; we suppress the arguments of  $J$  when no confusion arises. The corresponding parameter gradients of the two branches are

$$g_{\text{NFT}}^{(i)} = 2\beta^2 J^\top \mathbf{P} \left( v_\theta - Z_{\text{NFT}}^{(i)} \right), \quad (41)$$

$$g_{\text{CR}}^{(i)} = 2\lambda_{\text{CR}} t^2 J^\top \mathbf{P} \left( v_\theta - Z_{\text{CR}}^{(i)} \right), \quad (42)$$

where the  $2\beta^2$  prefactor in  $g_{\text{NFT}}^{(i)}$  originates from  $v_\theta^- - v^{(i)} = -\beta(v_\theta - Z_{\text{NFT}}^{(i)})$ , and the multiplicative  $t^2$  in  $g_{\text{CR}}^{(i)}$  is a structural consequence of writing the corrective loss in  $\mathbf{x}_0$ -space (Eq. (9)): the residual identity  $\hat{\mathbf{x}}_0^{(i)} - \bar{\mathbf{x}}_0^+ = -t(v_\theta - Z_{\text{CR}}^{(i)})$  converts the  $\mathbf{x}_0$ -residual into a velocity-residual, contributing a multiplicative  $t$  to the per-sample gradient and hence a  $t^2$  multiplicative factor in its covariance. Throughout we further assume the Jacobian block-alignment condition

$$\mathbf{P} K (I - \mathbf{P}) \approx 0, \quad (43)$$

which prevents off-mask residual noise from leaking into on-mask parameters through shared  $J^\top$ . The condition is approximate but reasonable for the DiT velocity field used here, whose attention-mediated structure is locally aligned with the violation mask.

**Proposition 2** (Gradient variance reduction of the corrective branch). *Fix a common active projector  $\mathbf{P}$ . Under the across-history convention in Eq. (39) and the conditional independence  $\xi_{\text{EMA}} \perp \{v^{(i)}, \bar{\mathbf{x}}_0^+\} \mid x_t, t$ , the corrective velocity target satisfies the marginal-covariance identity*

$$\text{tr} \text{Cov} \left[ \mathbf{P} Z_{\text{CR}}^{(i)} \mid x_t, t \right] = \frac{1}{|\mathcal{P}|t^2} \text{tr} \text{Cov}_{\pi+(\cdot|y)}[\mathbf{P} x_0], \quad (44)$$

which diverges as  $\Theta(1/t^2)$  at small  $t$  because  $\bar{\mathbf{x}}_0^+ \perp x_t^{(i)} \mid y$  collapses the conditional onto the within-condition marginal. The corresponding parameter-gradient trace covariances of the two branches admit the exact decompositions

$$\text{tr Cov}[g_{\text{NFT}}^{(i)} \mid x_t, t] = 4\beta^2 \text{tr}(J^\top \mathbf{P} \text{Cov}[v^{(i)} \mid x_t, t] \mathbf{P} J) + 4\beta^2(\beta + 1)^2 \Sigma_\xi, \quad (45)$$

$$\text{tr Cov}[g_{\text{CR}}^{(i)} \mid x_t, t] = \frac{4\lambda_{\text{CR}}^2 t^2}{|\mathcal{P}|} \Sigma_0^+, \quad (46)$$

where  $\Sigma_\xi := \text{tr}(J^\top \mathbf{P} \text{Cov}[\xi_{\text{EMA}}] \mathbf{P} J) \geq 0$  and  $\Sigma_0^+ := \text{tr}(J^\top \mathbf{P} \text{Cov}_{\pi+(\cdot|y)}[\mathbf{P} x_0] \mathbf{P} J) \geq 0$ . Consequently the gradient-covariance gap obeys

$$\text{tr Cov}[g_{\text{NFT}}^{(i)} \mid x_t, t] - \text{tr Cov}[g_{\text{CR}}^{(i)} \mid x_t, t] \geq 4\beta^2(\beta + 1)^2 \Sigma_\xi - \frac{4\lambda_{\text{CR}}^2 t^2}{|\mathcal{P}|} \Sigma_0^+, \quad (47)$$

which is strictly positive whenever the EMA plug-in is noisy on  $\mathbf{P}$  ( $\Sigma_\xi > 0$ ) and  $t < t^* := \frac{\beta(\beta+1)}{\lambda_{\text{CR}}} \sqrt{|\mathcal{P}| \Sigma_\xi / \Sigma_0^+}$ . In particular, in the small- $t$  regime

$$\text{tr Cov}[g_{\text{NFT}}^{(i)} \mid x_t, t] = \Theta(1), \quad \text{tr Cov}[g_{\text{CR}}^{(i)} \mid x_t, t] = O(t^2), \quad (48)$$

so the corrective gradient covariance vanishes as  $t \rightarrow 0$  while the NFT gradient covariance retains the persistent EMA-plug-in floor  $4\beta^2(\beta + 1)^2 \Sigma_\xi$ .

*Proof.* Eq. (44) follows from Eq. (38): because  $\bar{\mathbf{x}}_0^+ \perp x_t^{(i)} \mid y$  and the within-group positives are independent of the negative rollout's own  $x_0^{(i)}$ , conditioning on  $(x_t, t)$  on the left collapses to the within-condition marginal on the right, and total covariance with the (assumed independent) EMA-plug-in noise leaves the identity unchanged. By Eq. (41),  $\text{Cov}[g_{\text{NFT}}^{(i)} \mid x_t, t] = 4\beta^4 J^\top \mathbf{P} \text{Cov}[Z_{\text{NFT}}^{(i)} \mid x_t, t] \mathbf{P} J$  since  $v_\theta$  is  $\theta$ -deterministic given  $(x_t, t, y)$ ; substituting Eq. (40) (whose right-hand side carries factors  $1/\beta^2$  and  $(\beta + 1)^2/\beta^2$ ) and taking the trace yields Eq. (45). By Eq. (42) the  $t^2$  factor in  $g_{\text{CR}}^{(i)}$  contributes a multiplicative  $t^4$  in  $\text{Cov}[g_{\text{CR}}^{(i)} \mid x_t, t]$ , and substituting Eq. (44) produces  $t^4 \cdot (1/(|\mathcal{P}|t^2)) = t^2/|\mathcal{P}|$ , hence Eq. (46). Eq. (47) follows by dropping the manifestly non-negative flow-matching term in Eq. (45); setting the right-hand side to zero and solving for  $t$  gives the threshold  $t^*$ . The asymptotic statement Eq. (48) follows because  $\text{Cov}[v^{(i)} \mid x_t, t] = t^{-2} \text{Cov}[\mathbf{x}_0^{(i)} \mid x_t, t]$  with the rectified-flow posterior  $\text{Cov}[\mathbf{x}_0^{(i)} \mid x_t, t] = \Theta(t^2)$  as  $t \rightarrow 0$  (the posterior collapses onto  $x_t$ ), so the first term of Eq. (45) is  $\Theta(1)$ , the EMA floor  $\Theta(\Sigma_\xi)$  persists, and Eq. (46) is manifestly  $O(t^2)$ .  $\square$

**Interpretation.** Two distinct, complementary variance-reduction mechanisms compose at the gradient level. First, the corrective branch is structurally EMA-free: regressing toward a positive-side target rather than a reflected EMA plug-in eliminates the  $4\beta^2(\beta + 1)^2 \Sigma_\xi$  plug-in floor that the negative branch of NFT-style estimators carries by construction (Eq. (45)). Second, although the corrective velocity target itself has a  $\Theta(1/t^2)$ -divergent per-step covariance (Eq. (44))—a direct consequence of  $\bar{\mathbf{x}}_0^+ \perp x_t^{(i)} \mid y$ , which prevents the flow-matching posterior from collapsing the marginal positive dispersion—the  $t^2$  weighting induced by writing the loss in  $\mathbf{x}_0$ -space (Eq. (9)) injects a  $t^4$  factor into the gradient covariance (Eq. (46)), turning the divergent target into an  $O(t^2)$  vanishing gradient floor. Aggregation over  $|\mathcal{P}|$  within-group positives further shrinks the residual gradient covariance by exactly  $|\mathcal{P}|^{-1}$ . Both effects rely only on the rollout group's i.i.d. structure under shared conditioning  $y$  and on the loss being formulated in  $\mathbf{x}_0$ -space; no covariance-dominance or matching-Lipschitzness condition is required.

**Takeaway.** CreFlow's corrective branch achieves a strict reduction in the parameter-gradient trace covariance for all sufficiently small  $t < t^*$ , and asymptotically dominates the NFT branch as  $t \rightarrow 0$ . Two complementary, unconditional mechanisms drive this reduction. First, dispensing with the reflected EMA plug-in eliminates the persistent  $\Theta(\beta^2(\beta + 1)^2 \Sigma_\xi)$  EMA floor that the NFT branch retains (Eq. (45)). Second, the  $\mathbf{x}_0$ -space loss formulation (Eq. (9)) supplies an automatic  $t^2$  down-weighting of the corrective gradient (Eq. (46)) that perfectly cancels the  $\Theta(1/t^2)$  divergence of the marginal-positive target covariance, leaving an  $O(t^2)$  residual that is further shrunk by  $|\mathcal{P}|^{-1}$  via the within-group positive mean. Both reductions follow from the rollout group's i.i.d. structure under shared conditioning  $y$ , with no additional architectural or empirical assumptions.

## A.6 Discussion of assumptions

**Reward-local mask assumption.** Equation (22) says that off the violation mask, positive and negative rollouts have the same conditional velocity in expectation. This is the formal version of the credit-assignment intuition behind the compositional monitor: a binary failure should be attributed to the entities and frames appearing in the violation trace, not to the entire video. The assumption is not exact at the pixel level, because rendering jitter and background changes can occur off mask. The KL anchor and the pretrained video prior are therefore still necessary to prevent irrelevant coordinates from drifting. Operationally, the  $|\mathbf{M}|/|\Omega| \in [1\%, 5\%]$  sparse-support observation of §1 is a direct consequence: violation traces concentrate on the few entities and frames that actually disagreed with the predicate, not on the bulk of the latent.

**Population-level mask assumption (Assumption 1).** Strictly speaking, the empirical mask  $\mathbf{M}$  in Eq. (6) is a deterministic function of the within-group un-noised rollouts  $\{\mathbf{x}_0^{(j)}\}_{j=1}^N$  (through the LTL violation traces and the SAM3 atlases) and is therefore random when one conditions on  $(x_t^{(i)}, t)$  alone. Factoring  $\mathbf{M}(\omega)$  out of  $\mathbb{E}[\cdot | x_t, t]$  in the proofs of Theorem 2 and Lemma 1 therefore requires the population-level reading of  $\mathbf{M}$  stated in Assumption 1: at the population level we identify  $\mathbf{M}$  with the reward-locality support that already appears in Eq. (22), so  $\mathbf{M}$  is treated as  $\sigma(x_t, t)$ -measurable and the empirical  $\mathbf{M}$  of Eq. (6) is read as a Monte Carlo estimator of that fixed support. This is a natural population counterpart of the reward-local mask assumption above: both express the same credit-assignment principle—that off-mask coordinates carry no clause-level disagreement—in their respective regimes. The assumption is unrelated to the variance-reduction story of §A.5, which is fully unconditional.

**Mask validity across noise levels.** We emphasize that  $\mathbf{M}$  is a mask on the *coordinates of the velocity tensor*, not on the *content of  $x_t$* . Reward locality (Eq. (22)) is a population-level statement about the conditional velocity fields  $v^\pm, v^{\text{old}}$  at every  $(x_t, t)$ , independent of how informative  $x_t$  is about  $x_0$ . In particular, at high noise where  $x_t \approx \epsilon$  becomes uninformative about  $x_0$ , the conditional positive and negative velocities both collapse on  $\bar{\mathbf{P}}$  to  $v^{\text{old}}$  (off-mask reward locality), while on  $\mathbf{P}$  they coincide with the marginal-prototype velocity  $\bar{v}^+$  (Lemma 1). Masking therefore remains exactly the right localization across the entire  $t \in [0, 1]$  trajectory, and the mask need not be  $t$ -dependent.

**Within-group positive mean as the corrective target.** The corrective branch uses the empirical mean  $\bar{\mathbf{x}}_0^+ = |\mathcal{P}|^{-1} \sum_{j \in \mathcal{P}} \mathbf{x}_0^{(j)}$  of within-group positives instead of any selected single positive. Because the within-group positives are i.i.d. from  $\pi^+(\cdot | y)$  and independent of the negative’s noised state  $x_t^{(i)}$  given  $y$ , the conditional first moment of  $\bar{\mathbf{x}}_0^+$  is the marginal positive mean  $\mathbb{E}_{\pi^+(\cdot | y)}[x_0]$  rather than the flow-matching conditional mean  $\mathbb{E}_{\pi^+}[x_0 | x_t, t]$ . Lemma 1 therefore states the population target as the marginal-prototype velocity  $\bar{v}^+(x_t, t) = (x_t - \mathbb{E}_{\pi^+(\cdot | y)}[x_0])/t$ , which agrees with the flow-matching positive velocity  $v^+$  at high noise and supplies a  $t$ -uniform marginal-positive bias at finite  $t$ . The corrective branch should therefore be read as a distributional anchor toward  $\pi^+$ ’s marginal, not as a flow-matching estimator of  $v^+$ ; its complementarity with the credit-aware NFT branch (which carries the  $t$ -dependent  $v^+$  pull) is the mechanism by which the joint update ends up positively oriented along  $\Delta$  in expectation. Aggregation also shrinks the within-step target covariance by a factor of  $|\mathcal{P}|^{-1}$  relative to any single-positive variant (Eq. (44)); after multiplication by the  $x_0$ -space loss’s  $t^4$  gradient weighting, this  $|\mathcal{P}|^{-1}$  factor carries through to the corrective gradient covariance Eq. (46). The only residual statistical assumption is that  $|\mathcal{P}| \geq 1$  within a group, which the credit-aware NFT branch already requires for the violation-trace mask  $\mathbf{M}$  to be non-degenerate.

**KL term.** The KL regularizer generally moves the fixed point. Only under the local quadratic approximation of Eq. (27), and only when  $v_{\text{ref}} = v^{\text{old}}$ , does it simply shrink the coordinate-wise step without rotating the update direction. We therefore state the full weighted optimum of Proposition 1 with the KL term included, rather than claiming that KL “does not move” the fixed point.

**Gradient-level SNR.** By Theorem 2 the credit-aware NFT loss has zero gradient on off-mask coordinates, and under reward locality (Eq. (22)) the off-mask sample noise from either branch has zero population mean, so masking is unbiased. Translating this into a gradient-level statement at the parameter level additionally requires the Jacobian block-alignment condition Eq. (43) of §A.5, which prevents off-mask residual noise from leaking into on-mask parameters through shared  $J^\top$ . For the flow-matching DiT architecture used in this work, spatial-temporal parameter sharing is weak across

the mask boundary because the mask is a function of action-relevant content that the attention layers localize, so the approximation holds well in practice.

**Corrective-reflow gradient variance.** The variance-reduction claim of §A.5 is stated at the parameter-gradient level rather than at the velocity-target level, and is fully unconditional under the rollout group’s i.i.d. structure. The corrective velocity target  $Z_{\text{CR}}^{(i)}$  has a  $\Theta(1/t^2)$ -divergent per-step covariance at small  $t$  (Eq. (44)), because  $\bar{\mathbf{x}}_0^+ \perp x_t^{(i)} \mid y$  forbids the flow-matching posterior from collapsing the marginal positive dispersion; we make no claim of variance reduction at the target level. At the gradient level, however, the  $\mathbf{x}_0$ -space formulation of the corrective loss (Eq. (9)) injects a  $t^2$  down-weighting that converts this divergent target into an  $O(t^2)$ -vanishing gradient floor (Eq. (46)), while the NFT-branch gradient retains a persistent  $\Theta(\beta^2(\beta+1)^2\Sigma_\epsilon)$  EMA-plug-in floor (Eq. (45)). Aggregation over  $|\mathcal{P}|$  within-group positives further shrinks the residual corrective-branch gradient covariance by a factor of  $|\mathcal{P}|^{-1}$ . Proposition 2 therefore guarantees a strict reduction  $\text{tr Cov}[g_{\text{NFT}}] > \text{tr Cov}[g_{\text{CR}}]$  for all  $t < t^*$ , and the gap is  $\Theta(1)$  as  $t \rightarrow 0$ . No covariance-dominance or matching-Lipschitzness condition is required.

**Weighted-ERM generalization.** The corrective loss admits a one-parameter family of distributional-matching variants

$$\mathcal{L}_{\text{CR}}^{(w)}(\theta) = \lambda_{\text{CR}} \mathbb{E}_{i \in \mathcal{N}, t, \epsilon} \left[ \sum_{j \in \mathcal{P}} w_{ij} \|\mathbf{M} \odot (\hat{\mathbf{x}}_0^{(i)} - \mathbf{x}_0^{(j)})\|^2 \right], \quad \sum_{j \in \mathcal{P}} w_{ij} = 1, \quad w_{ij} \geq 0, \quad (49)$$

which are gradient-equivalent (by the squared-loss identity  $\sum_j w_{ij} \|x - x_j\|^2 = \|x - \sum_j w_{ij} x_j\|^2 + \text{const}$ ) to regression toward the weighted barycenter  $\sum_j w_{ij} \mathbf{x}_0^{(j)}$ . The uniform-weight choice  $w_{ij} = |\mathcal{P}|^{-1}$  used by the main method recovers Eq. (9); the kernel-weight choice  $w_{ij} \propto \exp(-\|\phi(\mathbf{x}_0^{(i)}) - \phi(\mathbf{x}_0^{(j)})\|^2/\tau)$  with bandwidth  $\tau$  recovers nearest-positive matching as  $\tau \rightarrow 0$  and the uniform mean as  $\tau \rightarrow \infty$ . We treat the kernel-weighted variant as an ablation (App. A.5) rather than the main method, since the uniform mean is the closed-form Monte Carlo estimator of the marginal positive prototype that drives Lemma 1 and Proposition 2.

**Summary.** CreFlow is best read as a localized corrective estimator for sparse-reward video diffusion RL. Violation masking projects the reward-induced learning signal onto the failure-relevant coordinates—retaining the full positive-flow pull along the reward-induced direction  $\Delta$  where the reward actually disagrees with the rollout, and exactly cancelling both branches’ off-mask sample noise under reward locality (Theorem 2, Eqs. (23)–(24)). The corrective loss replaces the reflected EMA plug-in with the within-group positive mean  $\bar{\mathbf{x}}_0^+$ , a distributional anchor whose conditional first moment is the marginal positive prototype  $\mathbb{E}_{\pi+(\cdot|y)}[x_0]$  on the violation mask (Lemma 1)—coinciding with the flow-matching positive velocity  $v^+$  at high noise and supplying a  $t$ -uniform marginal-positive pull at finite  $t$ —and whose  $\mathbf{x}_0$ -space loss formulation yields a strictly lower-variance *parameter-gradient* estimator at small  $t$  via an automatic  $t^2$  down-weighting and an additional  $|\mathcal{P}|^{-1}$  within-group shrinkage (Proposition 2). Under a local quadratic KL approximation, the active-coordinate update of CreFlow superposes a  $\Delta$ -aligned NFT pull and a  $\bar{\Delta}$ -aligned corrective pull on  $\mathbf{P}$ , with a coordinate-dependent step length on the violation-traced support (Proposition 1). Together, these two estimator-level interventions improve the bias–variance tradeoff of the sparse-reward update and explain the faster, more stable optimization observed empirically in §5.